Nanofabrication via Atom Optics

Jabez J. McClelland

Electron Physics Group

National Institute of Standards and Technology

Gaithersburg, MD 20899

USA

To appear in *Handbook of Nanostructured Materials and Nanotechnology*

To be published by Academic Press

I. Introduction.

Nanotechnology, because it is concerned with the construction of objects and devices a few nanometers in size, is dependent on the control of matter on the near-atomic scale. Remarkably, we have in recent decades developed tools for working in this regime despite the fact that it deals with objects more than seven orders of magnitude smaller than those encountered in everyday experience. Indeed, 30 years ago it seemed almost inconceivable that we could engineer materials with such precision. Nevertheless, exciting developments such as scanning probe microscopy, high-resolution electron microscopy, and self-assembled fabrication have contributed to the beginnings of a fast-developing field.

While we have seen a broad range of new nanoscale scientific studies and novel nanotechnologies emerge from the various techniques developed to date, there is still a great deal of progress to be made. Ultimately, it is desirable to have the ability to rapidly build any structure or array of structures with atomic precision using any material (i.e. any atoms) of choice. To reach this end, it is clear that simple refinement of existing techniques will not suffice. All of the tools currently in use, though they represent impressive advances over previous efforts, have fundamental limitations that prevent them from providing the ultimate in nanotechnology. To make further advances, it is important to continually examine completely different approaches to nanofabrication, with the hope that at least some of the fundamental obstacles will be circumvented with the introduction of new techniques.

It is in this spirit that nanofabrication with atom optics has become a subject of investigation in recent years. In this new technique, the motion of neutral atoms is controlled with nanoscale precision, allowing high-resolution structures to be constructed when the atoms are incident on a surface. The term atom optics is used because the ways in which the atomic motion is controlled have strong analogies in the ways that light rays are manipulated in light optics, or charged particle beams are steered and focused in electron (or ion) optics. In each case optical elements, such as lenses, mirrors, beamsplitters, diffraction gratings, etc. are constructed to transport a beam from an input (or object) region to an output (or image) region. Usually there is some form of magnification or demagnification during the process, yielding a desired pattern at the output.

As a new approach to nanofabrication, atom optics offers the possibility of several advantages over existing techniques. For one thing, the fundamental diffraction limit imposed on resolution, present in any process where one attempts to focus particles (whether photons, charged particles or neutral atoms), can be very small for atoms. This is because the De Broglie wavelength of a thermal atom is small—typically of order 10 pm—due to the relatively low velocity and large mass of an atom. Also, there is no resolution limit due to Coulomb repulsion (as is found in charged-particle lithographies) because the atoms are charge-neutral. Furthermore, atom optics can be used in both a direct deposition mode, where neutral atoms are focused by atom lenses into an extremely fine spot as they deposit onto a substrate, and also in a lithography mode, where focused atoms are used to expose a suitable resist material. In the direct deposition mode nanostructures can be fabricated in a clean, resist-free environment, with little or no damage to the underlying substrate (because of the low kinetic energy of the atoms). This is

important where issues of contamination and defect-free growth are critical. In the lithography mode, exposure of the resist is done with neutral atoms at thermal energies (the energy for resist exposure comes from internal atomic energy). Thus the process can be very localized, with very little scattering and resist penetration. In either mode, parallelism, which is advantageous when issues of fabrication speed and/or long-range spatial coherence are important, can be achieved with very high dimensional accuracy over a large area of the substrate using laser focusing of atoms in a laser interference pattern.

With all these potential advantages, it has become apparent that nanofabrication with atom optics could provide some new avenues for manipulation of matter on the near-atomic scale. This chapter will present a review of the basic concepts that are used for atom optical nanofabrication, and also a discussion of the progress to date in realizations of the techniques. Since the field is relatively new there is still a great deal to be learned, and many of the studies discussed represent the very first work in this field. As research continues, it is likely that more innovations will be forthcoming, and the full potential of the technique will be realized.

II. Manipulation of atoms.

In this section we discuss the various ways in which neutral atoms are manipulated, as a prelude to discussing atom optics and its use in nanofabrication. To begin with we examine the production and characteristics of neutral atomic beams, as these are a fundamental ingredient of atom optics. We then proceed with a discussion of the manipulation of atoms with electrostatic and magnetostatic fields, and lasers. It is worth noting at the outset that atoms, because of their charge neutrality, are much more difficult to manipulate than ions or electrons. For many years, the only manipulation of atoms that could be conceived of consisted of using apertures or slits to collimate a beam and perhaps a mechanical shutter to turn it on and off. We shall see below, however, that recent developments have introduced new ways to manipulate atoms, especially with lasers. These new techniques have paved the way for the establishment of the new concept of atom optics.

II.A. Atomic beams.

Beams of neutral atoms or molecules, since their first implementation in the early decades of the 20th century, have become a mainstay of both atomic and molecular physics experiments and also of thin-film deposition technologies. Much detailed understanding of their behavior has been developed over the decades, and this will only be summarized here. Several texts cover the subject in detail[1], notably the classic work by Ramsey[2], which has an atomic and molecular orientation, or reference [3] which treats the subject from a thin film point of view.

The most basic way to make a beam of atoms is by thermal evaporation in a vacuum system. Typically, a small cell or crucible of material is heated to the point where the vapor pressure is of the order 100 Pa (that is, around 1 Torr) and the evaporated atoms effuse from a small orifice into a vacuum system with pressure low enough (typically less than 10^{-7} Pa, or 10^{-5}

Torr) so that the mean free path of the atoms is of the order at least a meter or so (Fig. 1).

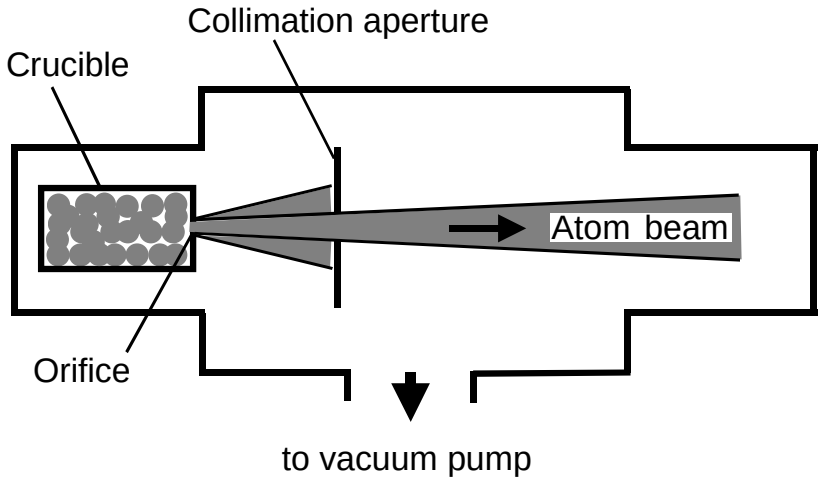

Figure 1 Schematic of a generic atom beam apparatus. In a vacuum chamber, heating a crucible containing the desired material produces atomic vapor. Atoms effuse through an orifice and are collimated by an aperture.

As the atoms emerge from the orifice, they fly in nominally straight lines across the vacuum system, eventually striking a substrate (or the vacuum chamber wall), where they stick or bounce depending on the local temperature and their particular chemical nature. If the pressure behind the orifice is not too high, so that few collisions occur as the atoms leave the aperture, the intensity distribution of the beam follows a cosine distribution, falling off as the cosine of the angle relative to the axis of the aperture. At a distance l from the orifice, the total flux on axis (in atoms per unit area per second) is given by

$$I = \frac{1}{4\pi}\frac{p\bar{v}a_0}{k_B T l^2}, \qquad (1)$$

where p is the vapor pressure of atoms in the cell, $\bar{v}$ is the average velocity, a_0 is the orifice area, k_B is Boltzmann's constant, and T is the cell temperature in Kelvin. Although a wide range of fluxes is in principle possible because of the very steep dependence of vapor pressures on temperature, as a practical matter for many atomic species typical fluxes a few centimeters beyond the orifice tend to be in the range of 10^{19} atoms-m^{-2}-s^{-1}.

The velocities of the atoms in the beam follow the Maxwell-Boltzmann thermal distribution based on the temperature of the cell, given by

$$F(v)dv = \frac{1}{2}\left(\frac{m}{k_B T}\right)^2 v^3 \exp\left(\frac{mv^2}{2k_B T}\right)dv, \qquad (2)$$

where $F(v)$ is the flux distribution, v is the velocity, and m is the atomic mass[4]. The most probable velocity for this distribution is $(3k_BT/m)^{1/2}$, which works out to be in the range 200 to 1000 m/s for most atomic species. The spread in velocities, as given by the root mean square of this distribution is $2(k_BT/m)^{1/2}$.

While thermal evaporation provides a good source for atomic beams of many atomic species, there are a few materials that present some difficulty because of their particularly low vapor pressures. Refractory metals such as W, Mo and Ta, for example, do not achieve significant vapor pressures until they reach temperatures of over 3000 ^{o}K. If beams of these materials are desired, other methods such as sputtering[5] or laser ablation[6] can be used. In sputtering, a beam of energetic ions is directed at a solid target of the desired material and atoms are dislodged collisionally. Laser ablation also uses a solid target, but a high energy, pulsed laser beam is focused onto the target, locally heating the material to a very high temperature and generating a plume of the desired atoms. Both of these methods have the advantage that very high fluxes can be obtained; indeed, they are often employed even for non-refractory materials if a very high flux is desired. One disadvantage, however, is that they tend to produce velocity distributions with most probable velocities corresponding to several electron volts of kinetic energy, which is much higher than the fraction of an electron volt typically seen in thermal sources. The widths of these distributions tend to be in the range of several eV as well, with long tails extending to high velocity.

Because atomic beams tend in general to have very broad velocity distributions, the implementation of any atom-optical system is potentially complicated by what amounts to chromatic aberration—that is, atoms with different velocities behave differently in the optical system. To minimize the effects of chromatic aberration it is often desirable to narrow the velocity spread in the atomic beam. One way of achieving this is to use a supersonic expansion[7]. This is done by increasing the vapor pressure of atoms in the crucible and making the orifice very small, so that a large number of collisions occur in the beam as it expands into the vacuum. These collisions, in combination with the rapid expansion of the gas of atoms, lower the effective temperature of the beam. The longitudinal velocity distribution is narrowed accordingly, in some cases to a width of about 10% of the mean velocity. The expansion can either be done using the vapor pressure of the atoms being evaporated, or alternatively using a carrier gas, typically a light noble gas such as helium or neon. The use of a carrier gas has proven particularly useful in combination with laser ablation[8] to make nearly monoenergetic beams of a wide range of atomic species.

Another way of narrowing the velocity distribution is by velocity selection. This is typically done by passing the atoms through a series of rotating slotted disks[9]. The slots are offset from each other so that for a given rotation speed of the disks, only one band of atomic velocities can pass through. With refinement of this technique, velocity monochromization (that is, reduction of the velocity spread) in the range of a few percent is attainable. However, a corresponding loss of flux is encountered, and the beam is by necessity pulsed.

II.B. Manipulating atoms with static electric and magnetic fields.

The interaction between a ground state neutral atom and an electrostatic field is extremely

small, and in most cases can be neglected completely. Whatever force does exist arises from an induced electric dipole moment in the atom and the presence of a gradient in the electric field. The induced dipole moment is $\boldsymbol{p} = \alpha \boldsymbol{E}$, where α is the polarizability of the atom and $\boldsymbol{E}$ is the electric field. The electrostatic energy of this dipole in the electric field is $W = -\boldsymbol{p}\cdot\boldsymbol{E} = -\alpha E^2$. Thus the force on the atom is given by $\nabla(\alpha E^2)$. To get an estimate of the size of this interaction, we note that typical atomic polarizabilities lie in the range from 0.2×10^{-50} farad-m^2 for helium, to 60×10^{-50} farad-m^2 for cesium. Considering a cesium atom in the presence of a typical laboratory electric field of about 1000 V/m with a gradient of about 10^6 V/m^2, the acceleration comes out to be about 5×10^{-15} m/s^2—a very small value. Larger accelerations might in principle be obtained, for instance, in the region near a very sharp point, where the gradient could be very high. An upper limit could be set by considering that field emission begins to occur at a field of about 10^9 V/m from a tip with about a 2 nm radius[10]. The gradient near the tip could be as high as 10^{18} V/m^2, leading to an acceleration of about 5000 m/s^2. This is a sizable acceleration, but an atom would have to be travelling very slowly to be affected by it because the region over which it acts, i.e. in the vicinity of the tip, is very small.

While the interaction with electrostatic fields requires an induced dipole moment, magnetostatic interactions can take advantage of the permanent magnetic dipole moment present on many atoms. The force arises from the energy shift $-\boldsymbol{\mu}\cdot\boldsymbol{B}$ felt by an atom with a net magnetic dipole moment $\boldsymbol{\mu}$ in the presence of a magnetic field $\boldsymbol{B}$. An atomic magnetic dipole moment occurs when the atom has non-zero angular momentum—either orbital, spin, or both. For example, a ground-state spin-1/2 atom has a magnetic moment with magnitude μ_B, the Bohr magnetron (9.274×10^{-24} J/Tesla). Atoms with more complex angular momentum configurations have magnetic dipole moments that depend on the details of the angular momentum coupling[11], but in most cases the values are usually within a factor of 3 of μ_B.

As with electrostatic fields, the force on the atom arises from a gradient in the magnetic field, i.e., $\boldsymbol{F} = \nabla(\boldsymbol{\mu}\cdot\boldsymbol{B})$. Considering again a cesium atom in its ground state, and taking a typical maximal laboratory gradient of 100 Tesla/m, we obtain an acceleration of 4400 m/s^2. Because the geometry of creating such a field gradient allows it to be applied over a fair amount of time, we see that a reasonable (though not huge) deflection of an atomic trajectory can be realized with a magnetostatic field.

II.C. Manipulating atoms with laser light.

While static electric and magnetic fields exert relatively weak forces on atoms, laser light, on the other hand, can be used to dramatically alter their trajectories. For example, light forces can be used to slow a thermal atom beam, compressing its velocity distribution, or even bring it to a complete stop[12]. For light forces to have a strong effect, however, a narrow-band laser must be used, and it must be tuned near an atomic resonance. If this can be done, two types of forces arise, one from the effects of spontaneous emission and the other from induced dipole effects[13].

Because of the wide range of applications for laser manipulated atoms, a number of

comprehensive reviews have been compiled on this subject. For more detailed information, the reader is referred to the reviews in references [14,15,16,17,18,19,20,21]. In what follows, we provide only a basic discussion of the origins of the effects.

II.C.1. Spontaneous force.

The spontaneous force arises from the scattering of photons in spontaneous emission. When an atom is exposed to near-resonant laser light, it will absorb photons and make transitions from its ground state to an excited state. In this absorption process the momentum carried by the photons, which points in the direction of the laser beam, is transferred to the atom (see Fig. 2).

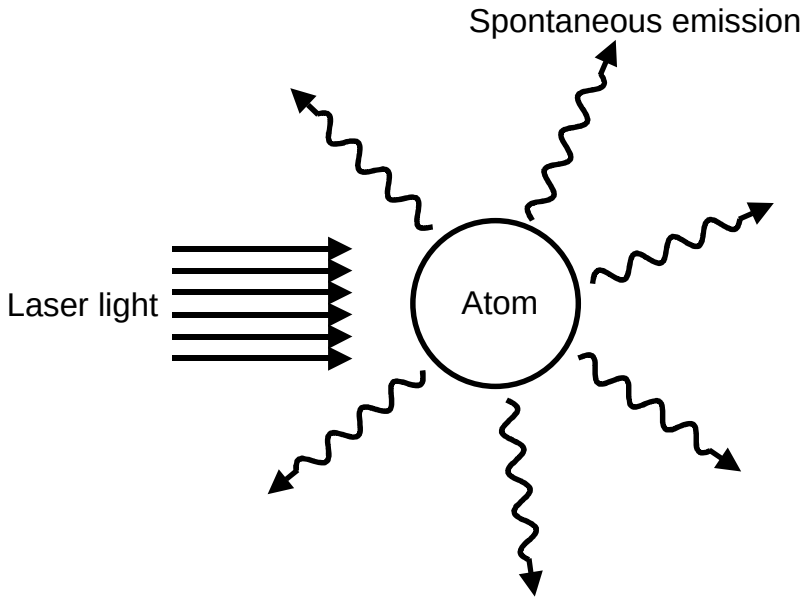

Figure 2 The spontaneous force exerted by laser light on an atom. Photons incident from one direction only are absorbed and re-emitted by spontaneous emission in all directions. The result, on average, is a transfer of momentum to the atom.

As the atom makes transitions back to the ground state it spontaneously gives off photons with momenta pointing in all directions. These momenta average to zero, so there is no recoil (on average) during the spontaneous decay. The result is that there is a net transfer of momentum to the atom in the direction of the laser beam. The magnitude of this momentum transfer depends on the number of photons scattered, each photon carrying a unit of momentum equal to $\hbar k$, where $k = 2\pi/\lambda$ is the wavenumber of the light. The rate of momentum transfer, or the force, depends on how frequently the atoms can give off a spontaneous photon, as governed by the atomic lifetime τ and the probability that the atom is in the excited state f_{ex}. Thus the force is given by

$$< F >= \frac{\hbar k \, f_{ex}}{\tau}. \qquad (3)$$

We note that the force in eq. (3) is an *average* force; the spontaneous emission process is of course random, and also leads to a diffusive component in the force, which can play an important role in some circumstances. The excited state fraction is given by

$$f_{ex} = \frac{\Omega^2}{2\Omega^2 + 4\Delta^2 + \Gamma^2} \qquad (4)$$

where in this expression, $\Gamma = 1/\tau$ is the atomic transition probability, Δ is the detuning of the laser from resonance, and Ω is the Rabi frequency, which contains information about the laser intensity I and the strength of the laser-atom interaction via $\Omega = \Gamma(I/2I_s)^{1/2}$, I_s being the saturation intensity associated with the atomic resonance[22].

Considering again the example of a cesium atom, we have a $6S_{1/2} \rightarrow 6P_{3/2}$ resonance at λ=852 nm, so $\hbar k = 7.8 \times 10^{-28}$ kg-m/s. The spontaneous lifetime of this resonance is 32 ns, so the force can be as high as 1.2×10^{-20} N if 50% of the atoms are in the excited state. This corresponds to an acceleration of 5×10^4 m/s^2—much larger than what is observed with electrostatic or magnetostatic fields.

As long as the atom and laser stay in resonance, the spontaneous force can be applied continuously, resulting in very significant changes in its motion. The resonance condition, however, can be affected by the Doppler shift, present when the atom has a velocity component toward or away from the laser beam. The Doppler shift is included in the force expression of eq. (4), by replacing the detuning Δ by a modified detuning $\Delta' = \Delta - \boldsymbol{k}\cdot\boldsymbol{v}$, where $\boldsymbol{v}$ is the atomic velocity. By evaluating $\boldsymbol{k}\cdot\boldsymbol{v}$ for typical parameters, it readily becomes clear that at thermal velocities the Doppler shift can be very significant relative to the natural linewidth of the atomic transition or the Rabi frequency, unless the angle between the atomic motion and the laser beam is very close to 90°.

The Doppler shift is especially important in experiments where atoms are being slowed by a counter-propagating laser beam. As the atoms slow, their velocity component along the laser beam changes by enough to shift them completely out of resonance very quickly. To counteract this effect, a number of approaches can be taken. For example, a spatially varying magnetic field can be used to keep the atoms in resonance by the Zeeman shift[23], the laser frequency can be varied in time ("chirped") to repeatedly slow one group of atoms after another[24], or very broadband laser light can be used[25].

So far our discussion of the spontaneous force has tacitly assumed only two atomic levels—the ground state and the excited state. If there are other states in the atom a possible pitfall arises as a result of what is referred to as optical pumping (see Fig. 3). Optical pumping occurs if somewhere below the excited state there is a metastable state that has even a small probability of receiving an atom by spontaneous decay. Over many excitation-decay cycles (required if the spontaneous force is to have a significant effect on the atomic motion), a sizeable fraction of the atoms can get trapped in the metastable state. As this happens, these atoms will stop participating in the spontaneous force process and become a potentially troublesome

background unaffected by the laser light.

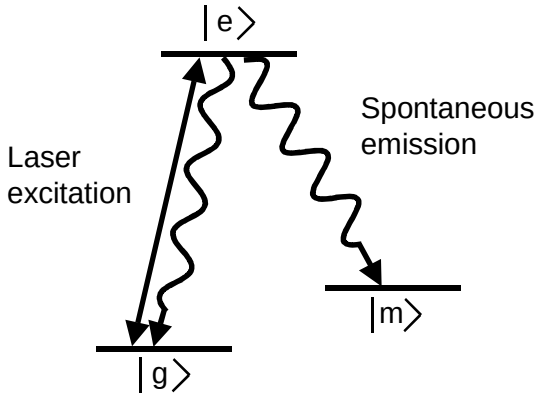

Figure 3 Optical pumping. A laser is used to excite an atom from the ground state |g> to the excited state |e>. While the atom is in the excited state, there is some probability that it will fall into the metastable state |m> by spontaneous emission. Once in |m>, the atom can no longer interact with the laser.

For example, in the case of sodium, the $3^2S_{1/2}$ ground state is split into two hyperfine levels separated by 1772 MHz. If the spontaneous force is exerted by tuning a laser from one of these levels to a hyperfine level of the excited $3^2P_{3/2}$ state, there is a finite probability that some atoms will decay into the other ground state hyperfine level. If nothing is done to prevent this, eventually all the atoms will be optically pumped into an off-resonance state and the spontaneous force will cease acting. Another example is chromium, where the spontaneous force can be applied by tuning 425-nm laser light from the 4^7S_3 ground state to the 4^7P_4 state located at 23500 cm^{-1} (~2.9 eV). About 8000 cm^{-1} (~1 eV) above the ground state lie the 4^5D metastable levels, which are weakly coupled to the excited state with a transition of about 6000 s^{-1}. Here, too, if the atoms are exposed to resonant radiation too long they will be lost and the spontaneous force will cease to have an effect.

In many cases, optical-pumping population traps can be remedied by adding additional laser frequencies to pump the lost atoms back into the ground-to-excited-state loop. For sodium, an acousto-optic or electro-optic modulator can be used to put sidebands on the main frequency, and for chromium, laser beams in the 660 nm range can be introduced. In some cases however, the problem can become quite difficult if, for example, there are no lasers available at the necessary wavelengths, or if there are too many metastable states. This latter situation occurs, for instance, if an attempt is made to apply the spontaneous force to molecules. Because of the manifolds of vibrational and rotational levels that exist in even the simplest molecular spectra, it is very unlikely for a given molecule to return to the original ground state and absorb more than one photon from the laser.

II.C.2. Dipole force.

The other significant form of interaction between an atom and laser light is the dipole force. In this case, the force arises from a shift in the energy of the atom induced by the presence

of the light field. If there is a spatial dependence in this shift, i.e. a gradient in the energy, there will be an associated force. This force can be many times larger than the spontaneous force because it does not rely on the rate of spontaneous emission, but rather on how strong the laser-atom coupling is and how steep a gradient in light intensity can be achieved. As will be seen below, it is the interaction of choice in a majority of the atom-optical implementations involving laser light.

To get some sense of the origin of the dipole force, a classical picture is helpful as a starting point. Consider the atom to be a charged harmonic oscillator (electron on a spring) with resonant frequency ω_o. One can then ask what happens when this atom is placed in a near-resonant oscillating electric field, that is, a laser field, with frequency ω. The effect of this field is to induce an oscillating electric dipole moment on the atom with magnitude that depends on the atomic polarizability and how close ω is to ω_o. The phase of the oscillating dipole relative to the phase of the electric field will vary from 0^o (in phase) to 180^o (out of phase) as ω goes from below the atomic resonance to above. Just as in the case for an atom in an electrostatic field, there will be an energy $-\boldsymbol{p}\cdot\boldsymbol{E}$ associated with the induced dipole in the presence of the external field. This energy will, however, be positive for detuning above resonance (positive detuning) and negative for detuning below resonance (negative detuning). Thus if the electric field has a gradient, the atom will feel a force away from high field strength for positive detuning, or toward high field strength for negative detuning.

While the classical description gives a good physical picture for the qualitative behavior of the dipole force, to correctly model the interaction a fully quantum treatment must be implemented. This can be done fairly easily via the dressed-state formalism for a two-level atom interacting with a monochromatic light field[26]. To determine the force on the atom in this approach the energy shift as a function of laser intensity is derived, and then a spatial derivative can be taken. The energy shift in the atom is obtained by forming the two dressed-atom wave functions |1> and |2>, each a linear combination of the ground and excited state. For positive detuning the state |1> consists of mostly the ground state, with an increasing admixture of the excited state as the laser intensity increases, and the state |2> is mostly the excited state with an increasing admixture of the ground state. The energies of states |1> and |2> are given by

$$E_1 = \frac{\hbar}{2}\left(\left[\Omega^2 + \Delta^2\right]^{1/2} - \Delta\right) \qquad (5)$$

$$E_2 = -\frac{\hbar}{2}\left(\left[\Omega^2 + \Delta^2\right]^{1/2} + \Delta\right) \qquad (6)$$

where $\Omega = \Gamma(I/2I_s)^{1/2}$ is the Rabi frequency and $\Delta=\omega_o-\omega$ is the detuning of the laser light from resonance. E_1 and E_2 are often referred to as light shifts of the atomic energy levels.

In situations where the laser is tuned relatively far from resonance, i.e., when $\Delta>>\Omega$, nearly all the population is in the state |1>, and this state is nearly identical to the ground state.

At this limit, the energy of the atoms in the field is approximately equal to $\hbar\Omega^2/(4\Delta)$. If the detuning is relatively small, however, the situation is a little more complex. Ignoring spontaneous emission, one simply has atomic populations in two states, with possible coherence between them, and the motion of the atoms is governed by the two distinct potentials[27]. Taking spontaneous emission into account, one can consider the limit in which the atom stays at rest while many spontaneous photons are emitted. In this case one can speak of a mean potential felt by the atoms, weighted by their relative populations in |1> and |2>. This potential is given by[26]

$$U = \frac{\hbar\Delta}{2}\ln\left(1+\frac{2\Omega^2}{\Gamma^2+4\Delta^2}\right) \qquad (7)$$

We note that in the limit $\Delta >> \Omega$, the expression for U approaches the same limit as equation (5), i.e., $U \cong \hbar\Omega^2/(4\Delta)$.

While the potentials given in eqs. (5) and (7) provide a simple basis for calculating the effects of a light field on the motion of an atom, often the real situation is more complicated. Most atoms are not two-level atoms, since at a minimum they will have some magnetic sublevels in the ground or excited state (or usually both). Considering that the laser light will have some definite polarization state, one must take into account which transitions between magnetic sublevels are allowed by optical selection rules and what their relative strengths are, as governed by the Clebsch-Gordan coefficients. The dressing of such a multilevel atom is possible, and it leads to an array of potentials. each associated with a state that is a linear combination of the various magnetic sublevels of the undressed atom. The motion of the atom on these potentials can be calculated, but in practice this must be done numerically because there are too many level populations and potentials to keep track of analytically.

The situation is further complicated when the atoms move across the potentials too quickly for the population to settle into the dressed levels, thereby inducing non-adiabatic transitions between the dressed levels. More complexity is introduced when spontaneous emission is taken into account, as this introduces random transitions between the dressed levels. To fully account for all these effects, and hence calculate exactly the motion of actual atoms in a light field, quantum Monte Carlo calculations are performed[28]. These consider the time evolution of the density matrix of the atoms, tracing many wave packets and allowing random spontaneous emission events to occur. After accumulating a large number of wave packets, the resulting distribution of atoms can be determined with fairly high accuracy. In the context of atom optics, these calculations find their most utility in providing confirmation of approximate models and modeling subtle experimental effects.

II.C.3. Laser cooling.

One of the most dramatic forms that laser manipulation of atoms can take is the cooling of an ensemble of atoms—that is, the reduction of the width of its velocity distribution. Laser

cooling can be remarkably efficient, reducing the effective temperature of a cloud of atoms to as low as 200 nK, or in some cases even lower. In addition to being a very useful tool for atom optics, laser cooling has a number of other applications, ranging from the development of very high precision atomic clocks[29] to the generation of a Bose-Einstein condensate[30].

The simplest form of laser cooling is referred to as Doppler cooling[31]. In this version, counterpropagating laser beams tuned below resonance are directed at the ensemble of atoms (see Fig. 4). If an atom in the ensemble has a velocity component toward any of the incoming

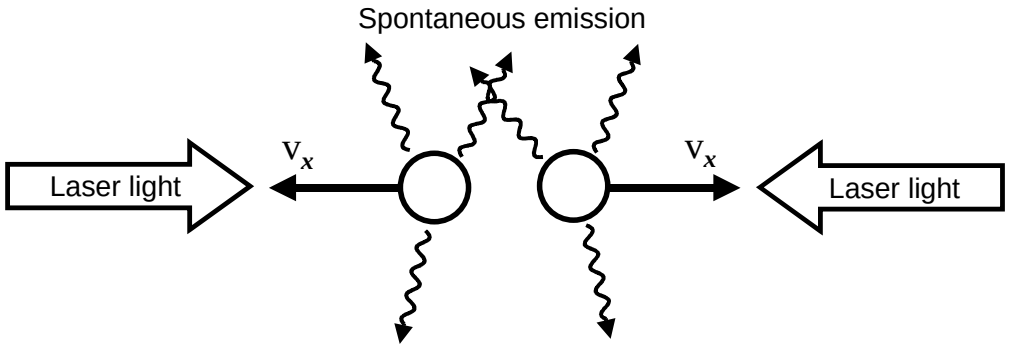

Figure 4 Doppler cooling. Counterpropagating laser beams, tuned below the atomic resonance, interact with a population of atoms with random velocities. Those atoms with velocity components toward one of the laser beams will be Doppler shifted closer to resonance, and hence will feel a stronger spontaneous force from that laser. Thus atoms feel a velocity-dependent force, which reduces the velocity spread of the population.

laser beams, it will see the laser frequency of that beam as being shifted higher due to the Doppler effect. Thus the incoming laser will appear to be closer to resonance and the atom will feel a stronger spontaneous force from this beam. The force will be greater the closer the frequency is shifted toward resonance, or equivalently the larger the velocity component toward the incoming laser beam is. The result is a velocity-dependent force in a region of space sometimes referred to as "optical molasses."[32] In such a region the atoms move exactly as if they are in a viscous medium that dissipates their kinetic energy and results in a narrower velocity spread; in other words they become cooled.

The limits of Doppler cooling are set by a balance between heating caused by continued spontaneous emission, which adds random momentum kicks to the atomic velocities, and cooling from the optical molasses. The minimum achievable temperature is given by[33]

$$k_B T_{\min} = \hbar\Gamma / 2 \qquad \text{(Doppler cooling)} \qquad (8)$$

where k_B is Boltzmann's constant and Γ is the spontaneous decay rate. For most atoms, this value is in the range of a few hundred μK.

Since the discovery of Doppler cooling, a number of new mechanisms that produce even colder atoms have been uncovered. Polarization-gradient cooling, in particular, has been shown to readily cool atoms below the Doppler limit[34,35]. In this form of laser cooling, use is made

of the potential hills created by the light shifts induced by the laser light. Atoms repeatedly climb these hills only to find themselves optically pumped to the bottom again—hence the term "Sisyphus cooling" is often applied, after the character in Greek myth who was forced to continually push a stone up a hill only to see it roll down again. The necessary configuration of potential hills is created by giving the counterpropagating laser beams different polarizations; for example they may be linearly polarized perpendicular to each other (lin ⊥ lin configuration), or one could be σ+ while the other is σ–. The other necessary ingredient, besides a laser tuned below resonance, is that the atom must have some magnetic sublevel structure in the form of at least two Zeeman levels in the ground state. When such an atom is placed in a lin ⊥ lin field, it can be viewed as moving on two light-shift-induced potentials, one for each Zeeman level. Each potential is sinusoidal in shape, but they are shifted by a half period relative to each other (see Fig. 5). As an atom in a given Zeeman level moves along the light-shift potential starting at the bottom of a hill, it must go up the potential and give up a corresponding amount of kinetic energy. At the peak of the hill, it is closest to resonance with the laser and hence has the greatest chance to be optically pumped to the other Zeeman level. If this pumping takes place, the atom finds itself at the bottom of the hill again because it is now on the other potential. As this process is repeated over and over, the atoms gradually lose energy and the ensemble can become cooled well below the Doppler limit. The minimum temperature obtainable in polarization-gradient cooling is conveniently expressed in terms of the recoil energy $E_R = \hbar^2 k^2/m$, which is the kinetic energy associated with the absorption and emission of a single photon. The smallest values seen experimentally are in the range of $10E_R$ to $15E_R$, and these are reasonably well explained by detailed theoretical calculations[36].

While it may seem that the recoil limit would represent an absolute minimum for any laser cooling process, recent research has shown that even this limit can be surpassed. Two schemes of interest that have demonstrated sub-recoil velocity spreads have been velocity-selective coherent population trapping (VSCPT)[37,38] and stimulated Raman cooling[39]. Both these processes are not, strictly speaking, cooling processes, but rely instead on creating a situation in which atoms can fall into a state that for a very narrow velocity range does not interact with the laser. By repeatedly giving atoms a chance to fall into this state, population can be accumulated with a very narrow velocity spread.

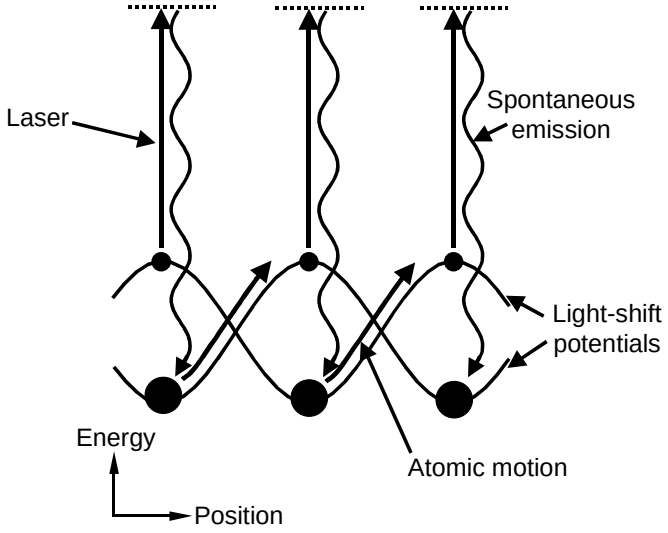

Figure 5 Polarization-gradient cooling. In a lin ⊥ lin laser field, an atom with two Zeeman levels in the ground state experiences two sinusoidal light-shift potentials offset by one-half period. As the atoms move along these potentials, optical pumping from one potential to the other occurs more readily at the peaks because the laser is red-detuned. Thus atoms are forced to travel "uphill" more frequently, resulting in a net loss of kinetic energy.

In VSCPT use is made of a coherent superposition of two degenerate ground states coupled through an excited state in a "Λ-configuration" (see Fig. 6a). Such a configuration is realizable, for instance, with the metastable helium 2^3S_1-2^3P_1 transition, where the M=+1 and M=−1 sublevels of the 2^3S_1 lower state can be coupled to each other through the M=0 sublevel of the 2^3P_1 excited state [37]. The coherent coupling between the two M-sublevels is created by couterpropagating lasers of opposite circular polarization, which results in a superposition state that cannot absorb photons (i.e., is "dark") if the atom has translational momentum $\pm\hbar k$. Thus if atoms fall into states with momentum $\pm\hbar k$ during a random walk process, they will remain there without being heated by scattering photons. The result is an accumulation of atoms in two very narrow velocity bands around the velocities $+\hbar k/m$ or $-\hbar k/m$. Using this scheme, temperatures (referring now to the width of the velocity distributions around $\pm\hbar k/m$) well below the recoil limit have been observed.

In the stimulated Raman process, cooling below recoil is achieved by making use of the "recoil-less" nature of stimulated Raman transitions. This type of cooling has been demonstrated in sodium, where Raman transitions are induced between the F=1 and F=2 hyperfine levels by pulses of two counter-propagating laser beams differing in frequency by the spacing of the hyperfine levels (1772 MHz) (see Fig. 6b). By varying the frequency width, detuning, and propagation direction of the Raman pulses, all atoms except those in a very narrow velocity band around zero are transferred from the F=1 to the F=2 hyperfine level. From there they are optically pumped back to the F=1 level, in the process randomizing their velocity and giving them a chance to have zero velocity again. After several Raman pulse-optical pumping cycles, a population of very cold atoms is accumulated, and this has been shown in one dimension to have

a velocity spread as small as 1/10th the recoil limit[39].

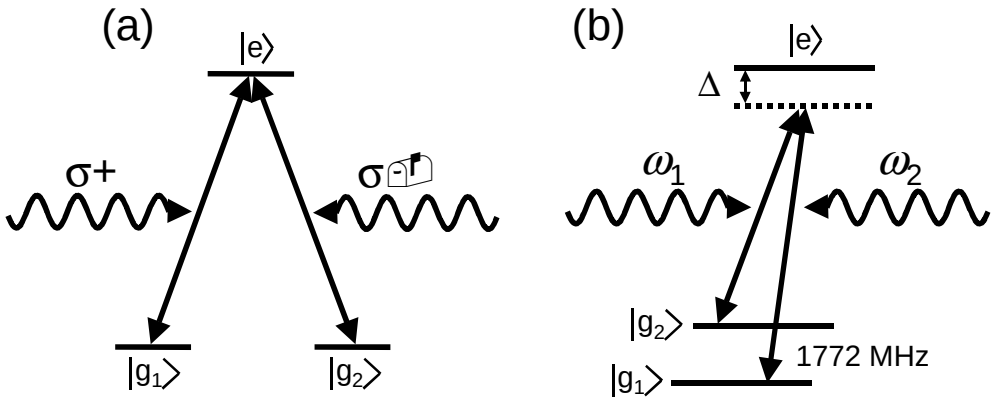

Figure 6(a) Velocity-selective coherent population trapping (VSCPT). In a Λ-configuration, an atom with two degenerate ground states $|g_1\rangle$ and $|g_2\rangle$ interacts with counterpropagating σ+ and σ– laser beams via a single excited state $|e\rangle$. If the atom has momentum $\pm\hbar k$, a coherent superposition state results that cannot absorb photons. Over time atoms with momenta in very narrow ranges around $\pm\hbar k$ accumulate in the superposition state, resulting in cooled populations. (b) Stimulated Raman cooling. In a sodium atom, counterpropagating laser pulses with frequencies differing by the hyperfine splitting of the ground state (1772 MHz) generate Raman transitions with a detuning Δ from the excited state $|e\rangle$. By adjusting the frequency width, detuning, and propagation direction of the pulses, selective population transfer for only atoms with near-zero velocity can be achieved. The result is an accumulation of cold atoms in one of the hyperfine states.

II.D. Atom trapping.

Another important development involving the manipulation of atoms is atom trapping. Motivated in part by the opportunities for extremely high resolution spectroscopy, and also the study of collective effects such as Bose-Einstein condensation, there has been a great deal of research recently into ways to generate potential wells that will trap neutral atoms. While to date the trapping of atoms has not been employed in any form of nanofabrication, the degree of control over atomic motion that it affords suggests that applications might be forthcoming in the near future.

In principle, all the interactions discussed in the earlier part of this chapter can be put to use to trap atoms, with varying degrees of success. Generally speaking, because any interactions with neutral atoms tend to be weak, atom traps tend to be quite shallow. For this reason the study of atom traps has historically been intimately connected with the study of atom cooling. An atomic population must be made very cold before it will be confined by the types of potentials available for trapping.

While electrostatic fields are generally too weak to trap atoms, magnetostatic traps have been used with considerable success. Considering the energy $-\boldsymbol{\mu}\cdot\boldsymbol{B}$ of an atom with a magnetic

dipole moment • in a magnetic field ***B***, one can see that atoms whose moment is aligned along the field will have a minimum energy at a minimum in the magnetic field strength. Such a local magnetic field minimum can be produced in three dimensions in a number of ways. For example, a quadrupole trap for sodium atoms has been demonstrated using a pair of coils in a Helmholtz geometry, but with current flowing in opposite directions in the two coils (anti-Helmholtz configuration)[40]. This type of trap generates a magnetic field that increases linearly in all directions from a value of zero at the center, and hence can have a relatively narrow confinement. It has a disadvantage, however, in that very cold atoms can escape in a very small region around the zero of magnetic field at the center of the trap by flipping their spins (that is, they undergo Majorana transitions). Another scheme, demonstrated with spin-polarized hydrogen atoms[41], employs a "pinch"-type trap made from a superconducting quadrupole magnet for radial confinement and two auxiliary solenoids for axial confinement. Still another scheme uses six permanent magnets oriented along three mutually orthogonal axes around a region in such a way as to create a local minimum at the center and a quadratic dependence of the field in the radial direction. This arrangement has been used to trap lithium atoms with good efficiency[42].

Although magnetostatic traps are simple in concept, and are useable when no optical means are available (such as with hydrogen), by far the most popular atom trap has proven to be the magneto-optical trap, or MOT[43]. This trap makes use of the spontaneous force from resonant laser light to confine atoms. It relies on there being some magnetic sublevel structure in the atom, and also on the fact that $\sigma+$ light excites only $\Delta M=+1$ transitions while $\sigma-$ light excites only $\Delta M=-1$ transitions. The atoms are placed in a quadrupole magnetic field generated by a pair of coils in the anti-Helmoltz configuration, and irradiated with three pairs of counterpropagating laser beams along three mutually orthogonal axes (see Fig. 7). The restoring force necessary to keep the atoms in the center of the trap is generated by a combination of (a) a laser tuned below resonance, (b) opposite circular polarization in the counter-propagating laser beams, and (c) a radially increasing Zeeman-shift of the atomic energy levels due to the magnetic field. Referring to Fig. 7b, which shows the energy levels of an idealized $J=0 \rightarrow J=1$ atom along one dimension of the trap, we see that with a laser tuned below resonance the $M=+1$ state is Zeeman-shifted closer to resonance for negative positions, while the $M=-1$ state is Zeeman-shifted closer to resonance for positive positions. Thus for negative positions, the atoms will interact most strongly with the $\sigma+$ light, which is incident from negative to positive, and vice-versa for positive positions. The result is a restoring force that keeps atoms trapped at the minimum of the magnetic field.

Magneto-optic traps owe their popularity to their relative simplicity of construction and their relative robustness of operation. Typically, up to 10^8 atoms can be confined with peak densities of up to $\sim 10^{11}$ atoms/cm^3. An added advantage of the traps is that the negative detuning of the laser contributes some velocity damping to the force, and hence the atoms are cooled as well as confined while in the trap. Temperatures around 1 mK can be readily achieved, and with some care even sub-Doppler cooling is possible[44].

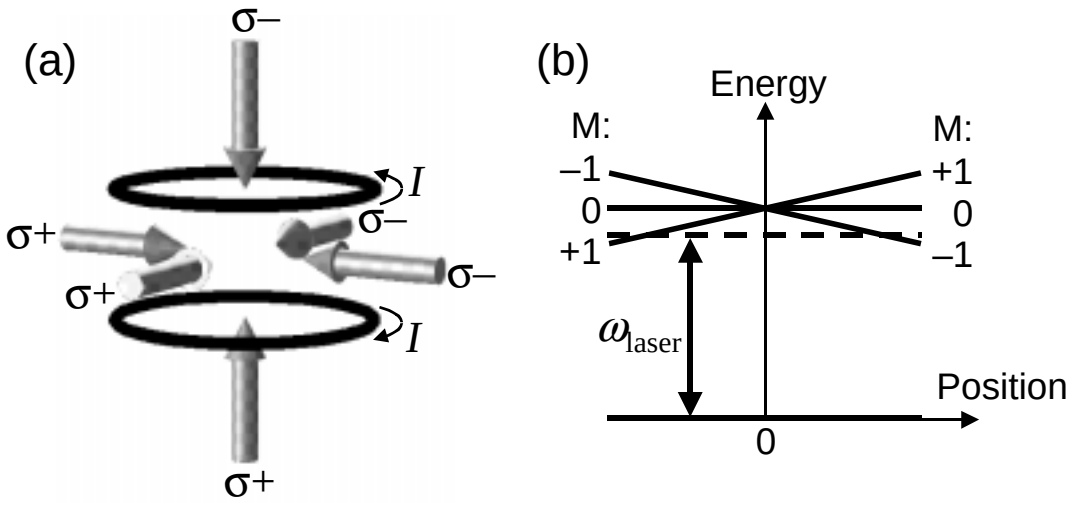

Figure 7 Magneto-optical trap (MOT). (a) A magnetic field that increases linearly from zero in all directions is produced by two coils with current I flowing in opposite directions (anti-Helmholtz configuration), and three pairs of oppositely-circularly-polarized laser beams counterpropagate through the center. (b) Energy of a $J = 0 \rightarrow J = 1$ atom in the presence of the magnetic field of a MOT. The magnetic sublevels $M = -1, 0, 1$ are shifted in opposite directions on opposite sides of the center. When the laser frequency ω_{laser} is tuned below resonance, atoms at negative positions are closer to resonance with the σ+ laser beam, while atoms at positive positions are closer to resonance with the σ– laser beam. Thus all atoms feel a net spontaneous force toward the center.

Atoms can also be confined with laser light alone. Making use of the dipole potential (see section II.C.2), a trap for sodium atoms has been demonstrated by tightly focusing a single red-detuned laser beam into a region of optical molasses[45]. The tuning below resonance of the trapping beam creates a dipole potential with a minimum at the highest laser intensity. Because the laser is a focused Gaussian beam, an ellipsoidal potential well is formed with its long axis along, and short axis transverse to, the laser beam. This concept has been further developed by making use of the fact that for large detuning, the potential depth is proportional to I/Δ and the excited state fraction is proportional to I/Δ^2. Thus a reasonable trap depth can be had with a very large detuning by using a very high laser intensity, all the while keeping the excited state population, and hence spontaneous emission and the associated heating, to a minimum. Such a trap has been demonstrated for rubidium atoms with a detuning of up to 65 nm below the D_1 resonance at 794 nm[46].

An intriguing example of dipole force atom trapping is the transverse confinement of atoms inside a hollow optical fiber. In the first demonstration of this[47], rubidium atoms were guided down the bore of a hollow optical fiber in which red-detuned laser light also propagated. The laser light in the fiber had a maximum along the axis, so the atoms felt a radially inward dipole force that prevented them from sticking to the fiber walls. Successful guiding was seen through a 31 mm length of fiber with a hollow core diameter of 40 μm. Recently, a similar guiding has been accomplished using blue-detuned laser light coupled into the shell of the hollow fiber[48]. This allowed the atoms to be confined in a low intensity region, thereby

reducing the effects of spontaneous emission.

II.E. Bose-Einstein Condensation.

One of the ultimate goals of atom cooling and trapping research has been the formation of a Bose-Einstein condensate. For many years it has been theoretically predicted[49] that a gas of atoms with the correct nuclear spin, if cold and dense enough, would undergo a phase transition, coalescing into a macroscopic occupation of a single quantum state with unique properties. Recently this phenomenon has been demonstrated for three different atoms: Rb[30], Li[50] and Na [51]. In each case a population of trapped atoms is cooled and compressed to the point where the predicted phase transition occurs, as evidenced by measurements on the spatial and velocity distributions of the atoms. In the case of Rb, the atoms were first trapped and cooled in a MOT. Then the MOT was shut off and the atoms were retrapped in a quadrupole magnetic trap that had an additional transverse rotating magnetic field component. The time orbiting potential, or TOP, created by this configuration prevented the atoms from undergoing Majorana transitions at the trap center. The trapped atoms were then subjected to evaporative cooling by turning on an RF field which selectively allowed hotter atoms to escape the trap. It was this evaporative cooling step that provided enough reduction in temperature and increase of phase space density for condensation to occur. The experiments with Li were similar, except the trap was purely magnetostatic, formed by six permanent magnets arranged to produce a magnetic field minimum at the center and a quadratic radial dependence. The Na experiments used a quadrupole trap like the Rb experiments, but the leak at the zero field point was sealed by focusing a far-off-resonant blue-detuned laser beam into the center of the trap.

Bose-Einstein condensation is of interest to atom optical methods for nanostructure fabrication mainly because of the type of atomic source it represents. As will be discussed in more detail below, thermal beams of atoms present some serious restrictions on what kind of atomic focusing can be achieved because of their spatial incoherence and broad velocity distributions. A Bose-Einstein condensate, on the other had, represents an extremely coherent group of atoms that could in principle be focused with much higher precision, or even diffracted to generate complex patterns. Just as the laser, which in a way represents a Bose-Einstein condensate of photons, has introduced a wide range of new optical applications, we can imagine that a Bose-Einstein condensate of atoms could open many new possibilities for atom optics. Although these possibilities may be far in the future, progress is presently encouraging, as evidenced by the very recent demonstration of a "atom laser" produced by coupling Na atoms out of a Bose-Einstein condensate[52].

III. Atom Optics.

We now turn to a more specific discussion of the types of atomic manipulation that can generally be grouped under the concept of atom optics. As the name implies, atom optics is concerned with producing "optical" elements for beams of neutral atoms. These optical elements include, for example, lenses, mirrors or gratings that manipulate atoms in ways analogous to the ways photons or charged particles are manipulated by similarly named objects in other forms of

optics. We give here a summary of some of the various types of atom optical elements that have been discussed in the literature. A number of reviews of this subject have also been published; in particular, references [17] and [53] are quite useful.

The analogy between atom optics and ordinary optics, which has both classical and quantum mechanical aspects, is a very useful concept. On the classical trajectory level, the analogy arises from the fact that the motion of any particles travelling predominantly in one direction and affected relatively weakly by a conservative potential can be treated with a paraxial approach. This allows the separation of longitudinal motion from transverse motion and makes the concept of lenses useful. On the quantum level, there is a fundamental similarity between the time-independent Schrödinger equation for a particle travelling in a conservative potential and the Helmholtz equation for an electromagnetic wave travelling in a dielectric medium[17]. Because these two take the same functional form, most of the results of scalar diffraction theory developed for light optics can be applied directly to atom optics. Thus many insights can be had into the behavior of atom optics just by considering the light or charged-particle analogue.

Another advantage to using the concept of atom optics is that the analysis of atom beam manipulation can be separated into the roles played by the object (that is, atom source) properties, and the optical system properties (see Fig. 8). One can then concentrate on two separate problems: (1) developing the best optical system, assuming the source to be (for example) a perfect plane wave, and (2) developing the best possible source. This simplifies the analysis and often points to where the weakness of a system is. Having separated the problem in this way, one can then go a step further and see if there is a way to modify the optical system to accommodate the atom source, such as is done for example in light optics with achromatic lenses.

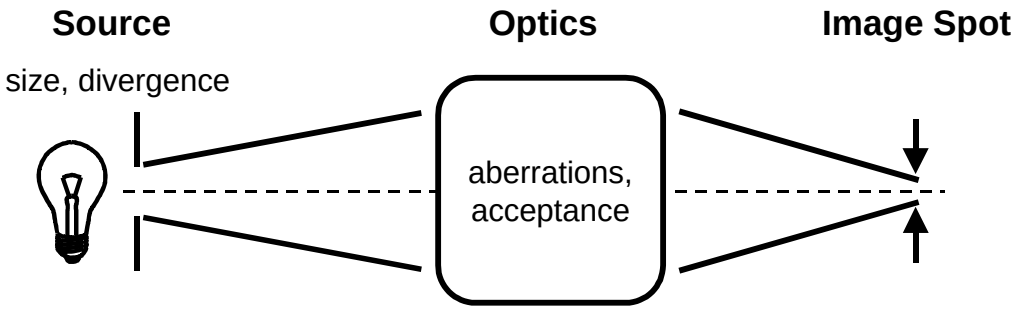

Figure 8 Components of an optical system, illustrating the separation into source and optics characteristics.

III.A. Atom lenses.

Because nanofabrication with atom optics is naturally concerned with concentrating atoms into nanoscale dimensions, atom lenses are of central importance for this field. Quite a few types of atom lenses have been discussed or demonstrated, utilizing a wide variety of atom manipulation methods. While so far the application to nanofabrication has only been done with a limited subset of the types of lenses available, it is nevertheless useful to consider what

possibilities exist, because future developments may broaden the field.

To construct an atom lens, the most important requirement is a force that is exerted radially toward the axis of the optical system with a magnitude proportional to the distance from the axis, i.e., $F=-kr$, where k is a constant (see Fig. 9). This is the necessary condition for Gaussian optics to hold, and is the situation in which pure imaging takes place according to the elementary laws of optics, for example the Gaussian lens law[54]

$$\frac{1}{s_1}+\frac{1}{s_2}=\frac{1}{f}, \qquad (9)$$

where s_1 is the distance from the object to the lens, s_2 is the distance from the lens to the image, and f is the focal length of the lens.

In general it is only necessary for the linear radial force dependence to hold in the vicinity of the axis of the optical system. In fact, nearly all optical systems deviate from linear dependence away from the axis, but as long as there is linearity near the axis these deviations can be treated as aberrations. If the radial force acts only over a short axial distance (compared to the focal length), the additional approximation of a thin lens can be made. If this is not the case, though, formalisms exist for treating the lens as a thick and possibly an immersion lens without undue complications.

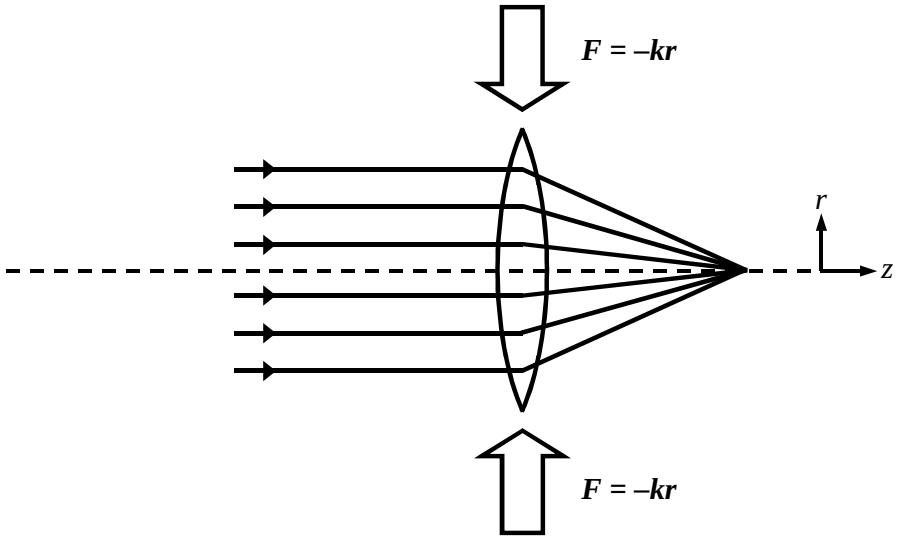

Figure 9 The essential property of a Gaussian lens: a transverse force F must be exerted that is proportional to the distance r from the axis, so that all initially parallel rays cross the axis at the same point.

The construction of an atom lens then reduces to the production of a linear radial force dependence in the vicinity of an axis. Such a force can be achieved for neutral atoms using

basically the same interactions that are used in atom traps – that is, either magnetostatic or optical forces[55]. Many arrangements of laser or magnetic fields that form atom lenses have been discussed in the literature; we discuss a few of them here to illustrate the variety of possibilities available.

III.A.1. Magnetic hexapole lens.

One of the earliest demonstrations of an atom lens utilized a magnetic hexapole field[56]. The radial dependence of such a field is quadratic near the center of the lens, resulting in the necessary linear dependence of the force on a spin-polarized atom. A recent demonstration of this type of lens[57] used NdFeB permanent magnet pole pieces arranged as shown in Fig. 10. Using a laser-slowed atom beam, this experiment showed imaging of a pattern of holes drilled in a screen placed at the object plane of the lens. The focal length of the lens is governed by the velocity v of the atoms and the second derivative of the magnetic field B at the center of the lens, and is given in the thin lens approximation by

$$f = \frac{mv^2}{2\mu_B \int \left(\partial^2 B / \partial z^2\right) dz}, \qquad (10)$$

where m is the mass of the atom. Typical focal lengths of 40-50 mm were obtained with Cs atoms slowed to 60-70 m/s and a magnetic field second derivative of $2.66 \times 10^4\ \mathrm{T/m^2}$.

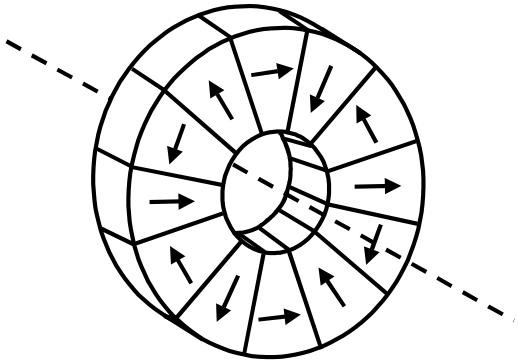

Figure 10 Pole configuration for the magnetic hexapole lens discussed in Kaenders *et al.*, Nature **375**, 214 (1995). Arrows indicate the direction of magnetization.

III.A.2. Coaxial laser lens.

The first demonstration of the use of laser light to focus atoms was done using a Gaussian, red-detuned laser beam co-propagating with a thermal sodium atom beam[58]. Because of the red detuning, the atoms felt a dipole force toward higher laser intensity and were therefore attracted toward the center of the laser beam. Concentration of the atoms was observed

by comparing the transverse atom beam profiles with the laser on and off. Using a 200 μm laser beam diameter, focusing of the atom beam to a spot size of 28 μm was achieved[59], demonstrating for the first time the concentration of atoms by laser light.

III.A.3. "Doughnut"-mode laser lens.

A major limitation on the spot size for atoms focused by a copropagating Gaussian laser beam is the diffusion of the atom trajectories caused by spontaneous emission. An alternative approach is to use a "doughnut"-mode, or TEM_{01}*, laser beam, which has a hollow center[60,61,62]. In this case the laser is blue-detuned so the atoms are concentrated in the lower intensity regions of the laser beams and hence experience less spontaneous emission. Calculations of the behavior of such a lens have shown that if the laser beam is brought to a diffraction-limited focus of approximately 1 μm, and if the atoms are constrained to travel through the center of this focus, focal spot sizes of 1 nm or less are in principle possible (see Fig. 11). An intriguing aspect of this "doughnut"-mode atom lens is that the axial dependence of the potential is such that the first-order (paraxial) equation of motion takes on exactly the same mathematical form as the equation of motion of an electron in a magnetostatic lens in the Glaser bell model[63]. This model, which allows an analytic solution to the equation of motion, has been analyzed in detail in the context of electron optics, so results can be transferred directly to the atom optical case. The result provides an opportunity to analyze an atom-optical lens in great detail, examining all the common aberrations such as spherical aberration, chromatic aberration and diffraction, as well as some unique ones such as spontaneous emission and dipole force fluctuations[62].

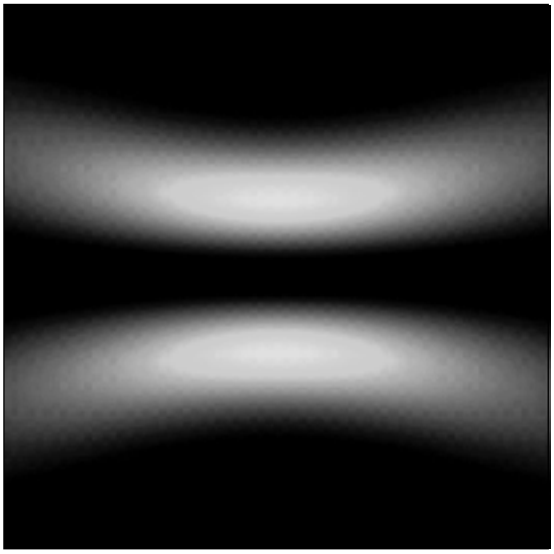

Figure 11 Schematic of atom focusing in a “doughnut”-mode (TEM_{01}*) laser beam. Atoms travelling coaxially through the focus of the laser beam feel a dipole force toward the axis, focusing them into a very small spot. Analysis of aberrations indicates that focal spots in the few-nm regime are possible.

III.A.4. Spontaneous force lens.

While the dipole force seems a natural choice for high-resolution focusing, it is also possible to focus atoms with the spontaneous force. Such a lens has been demonstrated using four diverging near-resonant laser beams aimed transversely at a sodium atomic beam from four sides (Fig. 12)[64]. The approximately linear force dependence in this case comes from the fact that the laser beams are diverging as they propagate toward the atom beam. Atoms travelling through this light field experience a higher laser intensity the farther away from the axis they are, and so the spontaneous force is greater (as long as the atomic transition is not saturated). With this lens, it was possible to create an easily discernible image of a two-aperture atomic source, demonstrating the imaging capability of the technique. The two oven apertures were 0.5 mm in diameter and the resulting image spot sizes were 1.3 mm in diameter. The spot size was found to be limited by chromatic and spherical aberrations, and also by the random component of the spontaneous force.

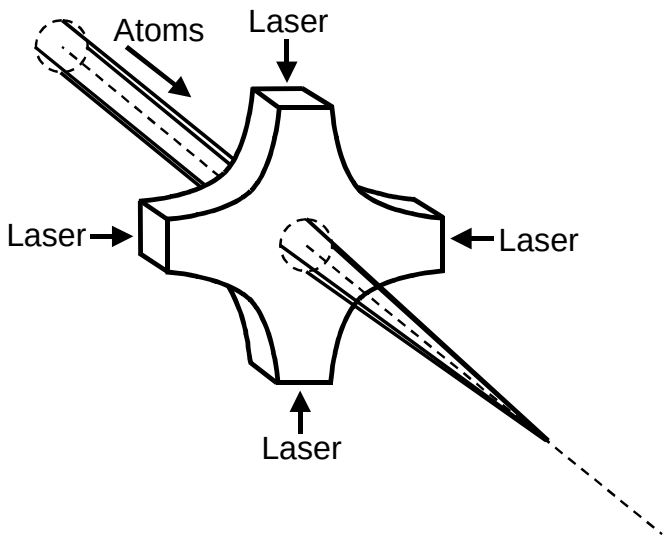

Figure 12 Spontaneous force lens. Four diverging resonant laser beams propagate transversely to the atom beam. Because the laser light becomes more intense as a function of distance from the axis, atoms feel a radially increasing spontaneous force, resulting in first-order focusing.

III.A.5. Large-period standing wave lens.

Another lensing technique demonstrated recently involved sending metastable helium atoms through a large period standing wave[65]. The large-period standing wave was formed by reflecting a laser beam, tuned just below the $2^3S_1 \rightarrow 2^3P_2$ transition at 1083 nm, at grazing incidence from a substrate placed transversely to the atom beam (see Fig. 13). The atom beam was apertured to 25 μm, so that it filled only a portion of a single antinode of the standing wave, which was 45 μm wide. Clear imaging, at unity magnification, of a 2 μm slit and also a grating with 8 μm periodicity was observed with this cylindrical lens. An image spot size of 6 μm was observed under optimal focusing conditions. The major contribution to this spot size was

considered to be diffraction, arising from the long focal length (28 cm) and small lens aperture (25 μm). Chromatic aberrations were held to a minimum because the atomic beam in this case was produced in a supersonic expansion. An additional interesting feature of this lens is that it was formed under conditions of relatively high intensity and small detuning. Ordinarily, spontaneous emission would be a major effect under these conditions, but in this case the transit time through the lens was too short for any significant amount to occur. Thus the atomic motion in the lens was governed by the two potentials given in eqs. (5) and (6), with a fair fraction (15%) of the atoms in the state that feels a repulsive potential.

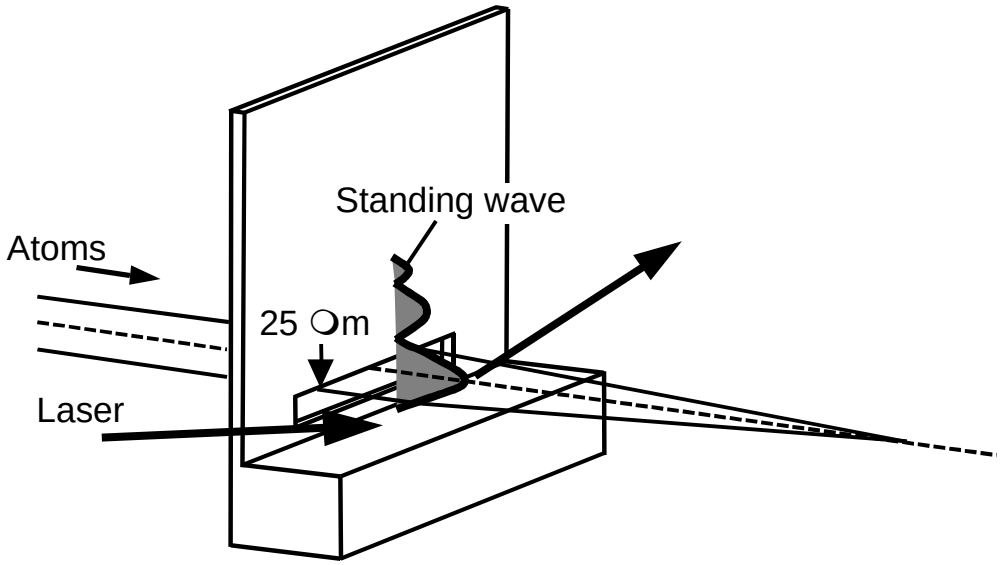

Figure 13 Large-period standing wave lens. A below-resonance laser beam reflects at grazing incidence from a substrate, creating a standing wave with a 45 •m-wide antinode. Atoms, apertured by a 25-•m slit aligned with the peak of the antinode, feel a dipole force toward the highest intensity, resulting in focusing.

III.A.6. Standing wave lens array.

An atom focusing technique that has seen a great deal of attention recently is the focusing of atoms in an array of lenses created by a laser standing wave. This technique has been used successfully for nanostructure fabrication[66,67,68,69], and will be discussed in detail later on in this chapter. The principle of the approach is to make use of each node of a near-resonant, blue-detuned laser standing wave as an individual lens, so that the entire standing wave acts as a large lens array (see Fig. 14). Near the center of the nodes of the standing wave the intensity increases quadratically as a function of distance from the node center. This intensity variation leads to a quadratically varying light-shift potential (as long as the excited-state fraction is low), and hence the force on the atom is linear and conditions are consistent with first-order focusing. Because of the high intensity gradient inside the node (the intensity goes from zero to full value in a fourth of an optical wavelength) it is relatively easy to get quite short focal lengths (of order a few tens of micrometers) with a standing wave lens, and hence small spot sizes, reaching into the

nanometer regime.

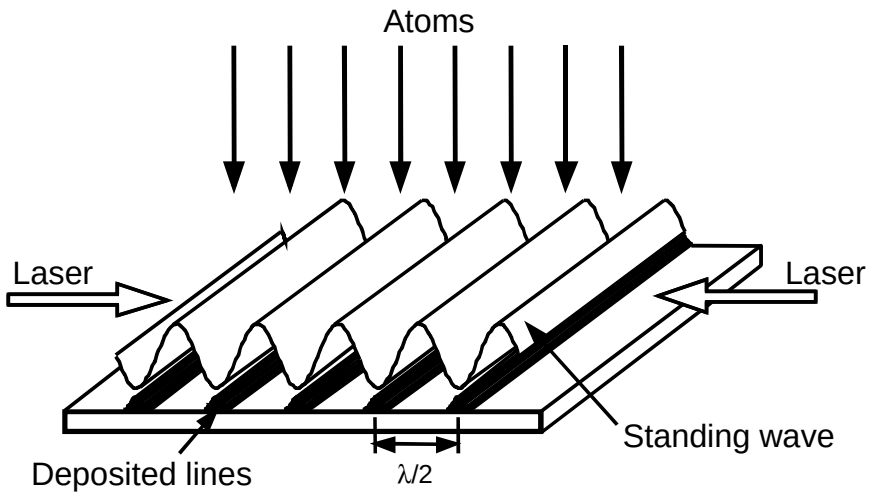

Figure 14 Standing wave lens array. An above-resonance laser standing wave propagates parallel to and as close as possible to a surface. Collimated atoms, incident perpendicular to the surface, are focused in each of the nodes of the standing wave by the dipole force. Nanometer-scale focusing has been demonstrated with this lens (see section IV.A).

III.A.7. Near-field lens.

Another recently proposed way to achieve nanometer-scale spot sizes makes use of the intensity pattern found in the vicinity of a small aperture irradiated by near-resonant red-detuned laser light[70]. In this scheme, atoms are passed through an aperture that is illuminated with light copropagating with the atoms (see Fig. 15). The aperture is typically made smaller than the optical wavelength, so the intensity pattern of the light on the far side of the aperture is dominated by near-field effects. Close to the aperture, the intensity falls off rapidly in both the radial and axial directions. The radial dependence of the intensity approaches a quadratic form near the axis, so again, the correct spatial variation of the light-shift potential for focusing is obtained. Because of the small size of the lens, short focal lengths can be obtained, and calculations involving the standard aberrations result in predicted spot sizes of 4-7 nm.

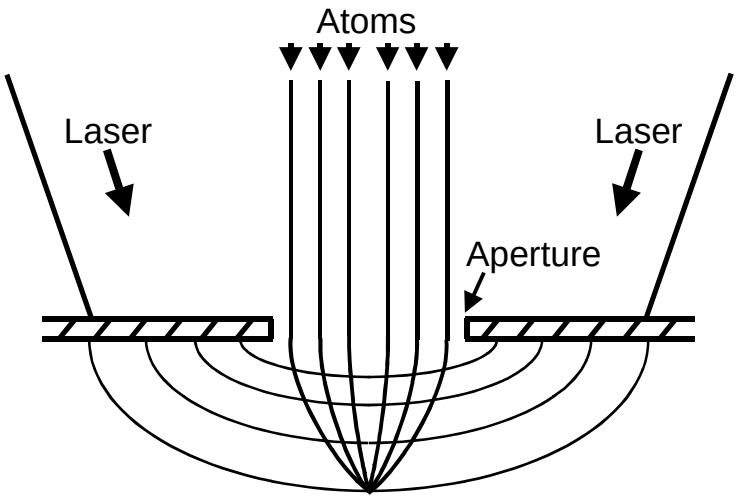

Figure 15 Near-field lens. Below-resonance laser light propagates through a sub-wavelength-size aperture. The longitudinally- and transversely-decaying transmitted laser light produces a light-shift potential that can focus atoms on the nanoscale.

III.A.8. Channeling standing wave lens.

While a laser standing wave can be used to construct an array of lenses for nanoscale focusing as discussed above, it is also worth noting that it can be used in a macroscopic sense as well. A recent demonstration has shown that a diverging sodium atom beam passing through a standing wave can be concentrated by making use of the channelling that occurs in the nodes of the standing wave[71]. In this arrangement, the laser intensity is high enough to cause the atoms to be confined by the dipole potential and oscillate within a node as they traverse the standing wave. As they emerge from the standing wave, their trajectories are concentrated into groups travelling either toward the axis or away from the axis. Those atoms approaching the axis can be considered to be focused.

III.A.9. Fresnel lens.

Although the bulk of atom lenses make use of magnetostatic or light forces, there is another type of focusing that has also been represented in atom optics. Fresnel lenses create focusing conditions by relying on a diffraction phenomenon. Typically a mask is fabricated that transmits incident radiation or particles in a pattern of concentric rings, the radii of which increase as the square root of the ring number, counting from the center out. Diffraction from this pattern of rings creates a spherical wavefront that is convergent on a spot beyond the lens, resulting in focusing (see Fig. 16). The focal length is given by $f = r_1^2 / \lambda_{dB}$, where r_1 is the radius of the innermost ring, and λ_{dB} is the De Broglie wavelength of the atoms. Such a lens has been demonstrated for atoms[72] using a free-standing Fresnel zone plate 210 μm in diameter microfabricated from gold. The plate had 128 zones and a first zone diameter of 18.76 μm. Focusing of metastable He atoms in the 2^1S_0 and 2^3S_1 states was observed, which occurred as a

result of diffraction due to the atomic De Broglie wavelength. The atoms were produced in a cooled supersonic expansion, so the velocity spread was narrow and the mean velocity was variable (by varying the source temperature). The De Broglie wavelength of the atoms was therefore well-defined, and was variable from 0.055 nm to 0.26 nm. Clear images of a single and a double slit were observed with approximately 1:1 imaging and a focal length of 0.45 m. The observed images of the 10 μm slit was 18 μm wide, in agreement with numerical calculations of the expected diffraction limit. While advantages of a Fresnel lens include no requirement for near-resonant laser light and hence no restriction on atomic species that can be focused, disadvantages include multiple focal lengths arising from multiple diffraction orders, and spot sizes limited to no smaller than the smallest feature that can be fabricated in the zone plate.

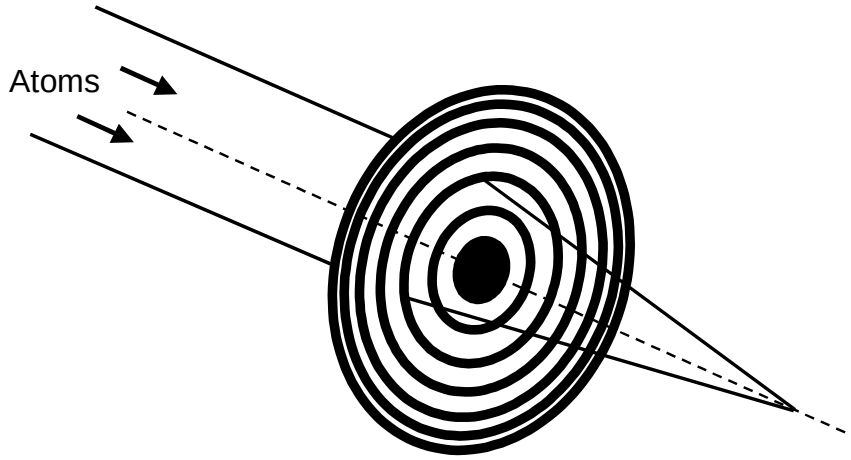

Figure 16 Fresnel lens. A transmission mask diffracts atoms to form a converging spherical wavefront, thereby focusing them. The mask consists of concentric rings that increase in radius as the square-root of the ring number, in accordance with the Fresnel zone formula.

III.A.10. Atom optical calculations.

Whatever particular geometry of laser or magnetic fields is chosen to make an atom optical lens, it is usually of interest to perform some calculations of the behavior of atoms in the lens to find out what focal lengths and resolutions might be expected. With the exception of the Fresnel lens, which must be treated with diffraction theory, most atom lenses can be treated quite successfully with a particle optics approach. Diffraction comes into play only in determining a limit on focal spot size. As long as the dimensions of the lens are large compared to the De Broglie wavelength, the spot size is well approximated by the diffraction limit formula used in conventional optics

$$d = \frac{0.61\lambda_{\mathrm{dB}}}{\alpha}, \qquad (11)$$

where d is the full-width at half maximum of the spot, λ_{dB} is the De Broglie wavelength, and α is

the convergence half-angle of the beam at the focus.

To trace the trajectories of atoms in a lens, the starting point is with the basic equations of motion derived from classical mechanics. In a cylindrically symmetric potential these reduce to

$$\frac{d^2r}{dt^2} + \frac{1}{m}\frac{\partial U(r,z)}{\partial r} = 0 \qquad (12)$$

$$\frac{d^2z}{dt^2} + \frac{1}{m}\frac{\partial U(r,z)}{\partial z} = 0 \qquad (13)$$

where r is the radial coordinate, z is the axial coordinate, m is the mass of the particle, and $U(r,z)$ is the potential. We note that eqs. (12) and (13) are also applicable in a one-dimensional focusing geometry, such as is found in a one-dimensional laser standing wave, with the substitution of the coordinate x for r. Thus all the following discussion also applies for this geometry.

One approach to analyzing an atom optical lens is simply to numerically integrate eqs. (12) and (13). This approach certainly gives useful information[73], but for motion that is generally axial it is often useful to eliminate time in these equations and write them as a single equation for r as a function of z. This is done by using the conservation of energy to reduce eqs. (12) and (13) to

$$\frac{d}{dz}\left[\left(1-\frac{U(r,z)}{E_0}\right)^{1/2}\left(1+r'^2\right)^{-1/2}r'\right]$$

$$+\frac{1}{2E_0}\left(1-\frac{U(r,z)}{E_o}\right)^{-1/2}\left(1+r'^2\right)^{1/2}\frac{\partial U(r,z)}{\partial r} = 0. \qquad (14)$$

To simplify eq. (14), it is very useful to make the paraxial approximation. This concentrates on trajectories that are not affected too greatly by the potential, i.e., those that are near the axis, and is made by taking the limit $r' << 1$ and $U(r,z)/E_0 << 1$. In the paraxial limit, eq. (14) reduces to

$$r'' + \frac{1}{2E_0}\frac{\partial U(r,z)}{\partial r} = 0. \qquad (15)$$

Eq. (15) provides a very simple equation that can often be solved analytically, or at least with minimal numerical assistance. This allows first-order lens properties to be derived, such as focal lengths, and principal plane locations if the lens is thick. Such an analysis is invaluable in determining the basic behavior of the lens in terms of the external parameters, such as magnetic field strength or laser intensity and detuning [62,74].

After the paraxial approximation is made, it is then possible to determine the spot size

limitations introduced by lens aberrations. Aberrations originate from the higher order terms in the expansion of equation (14), and also from any spread that may be present in the velocities of the atoms entering the lens (chromatic aberration). The effects of aberrations can be analyzed by taking the next-order terms in the expansion of eq. (14), as is done in conventional aberration theory[62]. Alternatively, it may be more straightforward to numerically solve eq. (14). This can be done by introducing the slope of the trajectory $\alpha \equiv dr/dz$ as an independent variable and separating the equation into two first-order equations:

$$r' = \alpha \qquad (16)$$

$$\alpha' = \frac{1+\alpha^2}{2(E_0 - U)}\left(\alpha\frac{\partial U}{\partial z} - \frac{\partial U}{\partial r}\right) \qquad (17)$$

Eqs. (16) and (17) can be solved readily with conventional numerical integration techniques.

Without going any further into the details of aberrations, we note only that in the types of atom lenses that have been analyzed so far, spherical aberration (which results from higher-order terms in the expansion of the potential about the axis) tends to be relatively minor. Thus in the absence of other aberrations, a diffraction-limited spot size can often be achieved. On the other hand chromatic aberration, arising from the velocity spread of the incident atoms, tends to be rather significant. One way to see this is to solve the paraxial equation of motion for a particular lens and derive the velocity dependence of the focal length. For an immersion lens the focal length is proportional to the velocity, and for a thin lens it is proportional to v^2 [74]. Since atom beams tend to have relatively broad velocity spreads, this velocity dependence can lead to large chromatic aberration effects. For this reason, research has been carried out on the possibility of an achromatic lens for atoms[75].

III.A.11. Focusing vs. concentrating.

Before moving on to discuss other atom optical elements, we mention briefly one more aspect of atom lenses. Because forces on atoms are generally weak, in practice atom lenses are often generated by fields that extend over some distance in the axial direction (that is, along *z*). In this situation, lenses are more often thick than not, and in many instances multiple crossovers can occur within an atom lens. In such a situation (the coaxial laser lens of section III.A.2 is a good example of this), the concept of focal length is less useful. The atoms are essentially "channeled" by the focusing field, and the lens acts more as a concentrator than a true lens, in the sense that a small spot can be generated but no image could ever be formed at the focus. If the purpose of a lens is to produce a very small spot of atoms, however, this is not necessarily a disadvantage and in many cases it can be an advantage. If the atoms are channeled in a lens, one is not relying on focusing at a particular focal point, but rather on the average effect of many oscillations within the lens. Thus the effects of velocity spread in the atom beam are drastically reduced and the tolerance for focal location is greatly increased. The final spot size is of course not as small as can be achieved with true focusing, but nevertheless, this technique can be used to

focus to nanometer-scale sizes[66,67,68,69].

III.C. Atom mirrors.

While atom lenses are the main optical elements of interest for nanofabrication with atom optics, there are other ways to manipulate atoms that parallel the methods of light optics. For example, atom mirrors have been the subject of some research recently. Here, the object is to coherently reflect a beam of atoms by generating a surface from which the atoms bounce specularly. Uses for such a mirror include reflective focusing elements, or cavities for storing atoms.

To make an atom mirror, efforts have concentrated on using the same sorts of forces as those employed for trapping and focusing. Using a real physical surface is not in general practical because the interaction with the surface will typically not be at all elastic or specular due to the complex processes that are involved, such as chemisorption, physisorption or phonon excitation[76]. Resorting to magnetostatic or laser forces, one is faced with the same limitations experienced with trapping or focusing, that is, the types of interactions available are generally rather weak. Thus it is unreasonable to contemplate redirecting the high-velocity atoms in a thermal beam though a large angle because their kinetic energy is much higher than any potential that could be generated. To realize an atom mirror, very slow atoms (such as those falling from an atom trap) must be used, or else the refection must be at grazing incidence.

Atom mirrors have been demonstrated with both magnetostatic and laser fields. In the case of magnetostatic fields, use has been made of the strong gradients found near the surface of a magnetic material with a periodic array of alternating magnetizations. The magnetic field in the vicinity of such a surface falls off exponentially with distance from the surface, creating a repulsive potential for atoms with spins parallel to the magnetic field direction.

Utilizing this approach, reflection of rubidium atoms has been demonstrated from a section of magnetic recording media on which a sine wave was recorded[77]. The frequency of the sine wave was such that the magnetization reversed with a periodicity of 9.5 μm. The Rb atoms were first captured in a magneto-optic trap (MOT) and then released, so their velocity was only that attained by falling in the earth's gravitational field, i.e., 0.7 m/s in this case. The potential barrier created by the magnetic field was sufficient to reflect suitably polarized atoms with (94 ± 8)% probability in this experiment.

Another approach to this same type of atom mirror employed a stack of alternatingly-magnetized sheets of the high coercive strength material NdFeB[78]. Using 18 1.04-mm thick sheets, a mirror was constructed that could reflect Cs atoms dropped from a MOT with (100 ± 2)% probability. Multiple bounces were observed, and the specular nature of the reflection was verified by observing the dependence of reflection angle on incidence angle.

The reflection of atoms from a light-shift potential was first proposed in 1982[79]. In this scheme, the reflective light field is produced by total internal reflection of a near-resonant laser beam from within a prism. The light field above the surface of the prism does not propagate, but has an intensity that decays exponentially with a characteristic length $\lambda/2\pi$, which is of order 100

nm. Because of the exponential decay over such a short distance, there is a large gradient in the light-shift potential and hence a fairly strong repulsive force if the laser is detuned below resonance.

Demonstration of the reflection of atoms from an evanescent wave has been carried out with either atoms dropped from a MOT, or with atoms incident at a grazing angle. The bouncing of dropped atoms has been observed with sodium[80], cesium[81], and rubidium[82]. Multiple bounces have generally been observed, although there are usually some losses with each bounce due to the transverse velocity components of the atoms. In addition, there has been some indication that diffuse scattering arising from surface roughness plays a significant role in this type of mirror[82].

The reflection of thermal atoms at grazing incidence from an evanescent wave has been demonstrated with sodium atoms at incident angles of up to 7 mrad[83], and with metastable argon atoms at angles up to 6.4 mrad[84]. In the latter case, improved reflection was obtained by using a surface-plasmon enhanced evanescent wave, which was obtained by applying a multilayer planar optical waveguide to the surface of the prism.

III.D. Diffraction of atoms.

In addition to focusing and reflecting atoms, a third atom-optical process that has been studied is diffraction. Diffraction of neutral atoms arises because of the basic quantum mechanical principle that any particle is described by a wave function that obeys Schrödinger's equation. The existence of this wave function means that the particle has a De Broglie wavelength $\lambda_{dB} = h/p$, where h is Planck's constant and p is the particle's momentum. The result is that diffractive wave phenomena exist for particles in analogy to the common diffraction effects observed with light. This analogy is made rigorous by the fact that in the presence of a conservative potential, the time-independent Schrödinger equation takes on a form identical to the form of the equation for the propagation of an electromagnetic wave in a dielectric medium[17]. Since the equation is the same, all wave phenomena that are predicted for light must occur as well for particles in an equivalent situation.

An important consideration in discussing diffraction effects with neutral atoms is the size scale set by the De Broglie wavelength. Large, easily observable diffraction effects will in general only be seen when the diffracting body has feature sizes in the same range as the wavelength, which is of order 10 pm for thermal atoms. Such a situation occurs, for example, in scattering atoms from the regular atomic array found on a single-crystal surface, where atom diffraction has actually been put to use as a diagnostic tool to observe surface structure[85]. Most atom optical versions of diffraction, however, are done with larger, man-made structures. Thus the diffraction effects are generally small, and observation is not easy due to the difficulty in obtaining a source of atoms with enough longitudinal coherence (i.e., narrow velocity spread) and transverse coherence (i.e., collimation), to see an effect.

The motivation for demonstrating atom diffraction has for a large part been the production of coherent beamsplitters for the construction of atom interferometers[86,87]. Focusing of atoms with a Fresnel lens has been observed (see Section III.A.9), and holography

via atom interference has been demonstrated (see below), but the bulk of research so far has concentrated on making use of the fact that diffraction is one of the few ways to coherently separate a beam of atoms into two or more paths. Direct application of atom diffraction to nanostructure fabrication has so far not been demonstrated; nevertheless, we discuss a few of the implementations here, since these techniques constitute an integral part of atom optical research and could possibly find application to nanostructure fabrication in the future.

The diffraction of atoms from physical structures has been demonstrated in several forms in addition to the Fresnel zone plate discussed above[72], where metastable He atoms were diffracted and focused. In the first demonstration, sodium atoms were diffracted on passing through a microfabricated grating with 200 nm spatial period fabricated in a free-standing gold membrane[88]. A clear diffraction pattern was observed with first order peaks at 85 μrad, using a highly collimated (10 μrad) atom beam produced in a supersonic expansion with $\Delta v/v = 12\%$. The pattern was observed by detecting atoms with a scanning hot wire detector located 1.5 m beyond the grating. A similar observation was made using a supersonic beam of metastable helium atoms with De Broglie wavelength 0.1nm diffracting from a gold grating with 500 nm period[89]. More recently, interesting near- and intermediate-field diffraction effects have been observed in diffracting potassium atoms[90] and sodium atoms[91] from a series of gratings.

Perhaps the most dramatic demonstration of atom-optical diffraction has been the generation of a recognizable pattern by diffracting atoms through a computer-generated, microfabricated hologram[92,93]. In this demonstration, metastable neon atoms were first trapped in a MOT and then released by a push from a near-resonant laser beam. The atoms fell through a screen that had an array of 500 nm-scale holes cut into it by microlithography, arranged in a pattern calculated to be the hologram of a desired image. After diffracting from the screen, the atoms were detected by a microchannelplate in the far field, where a clear image was observed (see Fig. 17). The transverse and longitudinal coherences of the atoms were kept high in this case because the atoms were launched from a trap, where their transverse and longitudinal velocity spreads were highly reduced. This experiment shows that the possibility of holographically imaging atoms is real, and opens up the possibility of fabrication of an arbitrary nanoscale pattern in the future.

There have also been a number of demonstrations of atom diffraction from gratings created by light force potentials. In this case there is not a particularly good match between the De Broglie wavelength (around 10 pm) and the grating period (typically half an optical wavelength, or about 300 nm), but the regularity of the period, the strength of the interaction, and ease of producing the grating with an optical standing wave have led to quite a few measurements.

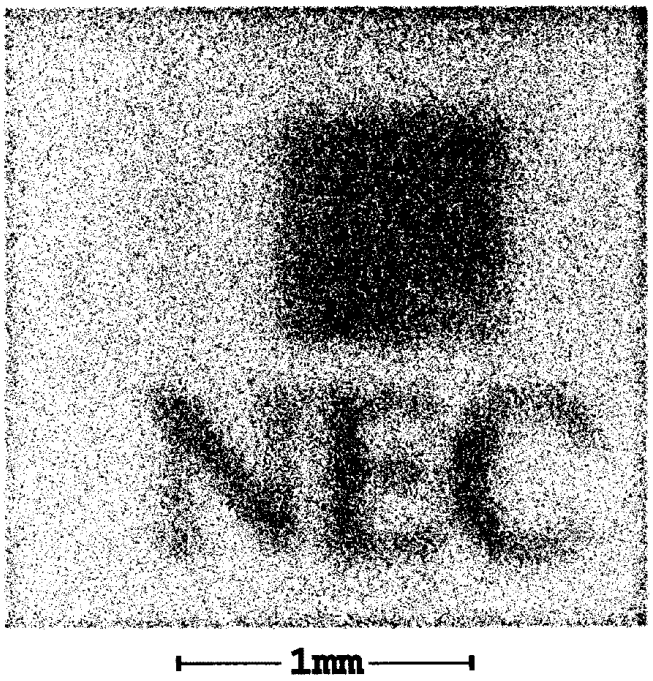

Figure 17 Image formed by diffraction of metastable Ne atoms passing through a computer-generated hologram fabricated as an array of 500 nm-scale holes in a 100 nm-thick silicon nitride film. The image was detected with a microchannelplate. (from M. Morinaga *et al*, Phys. Rev. Lett. **77**, 802 [1996]).

Diffraction has been observed from a standing wave in free space and also from a standing evanescent wave. The first demonstration of diffraction from a standing wave in free space was performed with sodium atoms produced in a supersonically-cooled beam collimated with two 10 μm slits separated by 0.9 m[94]. Using a red-detuned, narrow-waist standing wave with detunings ranging from 93 to 1116 MHz, and a variety of laser powers, clear diffraction peaks were observable. This work was further extended into the Bragg scattering regime, where the standing-wave grating was made with a broader laser beam waist[95]. Here the diffraction was restricted to angles that satisfy the Bragg condition, and good agreement was seen between predictions and experiment.

Subsequently, a number of examples of atom diffraction from a standing wave have been demonstrated. With emphasis on producing a large diffraction angle, metastable helium atoms have been diffracted from an optical standing wave in the presence of a magnetic field[96]. Here the shape of the light force potentials is modified by the magnetic field such that the grating is effectively "blazed" to emphasize higher-order diffraction. This sort of blazing of a light force grating for metastable helium has also been demonstrated without a magnetic field, making use of a pair of differentially-detuned standing waves offset in spatial phase by $\pi/2$[97].

Further demonstrations of atom diffraction from a standing wave light field have been performed with specific emphasis on creating an atom interferometer. Both metastable argon[98]

and also metastable neon[99] have been used with success, showing good diffraction effects in experimental arrangements suitable for measuring small angles.

To show that atoms can also be diffracted from a standing wave in the reflection mode, several experiments have been done using total internal reflection of a light wave from within a prism, much as was done for the atomic mirrors discussed in section III.C above. In this case two counter-propagating laser beams were superimposed to create a standing-wave grating along the surface that decayed exponentially in the direction perpendicular to the surface. The first demonstration of this effect was done with sodium atoms[100], with further work done using metastable neon atoms[101, 102].

III.D. Collimation and velocity compression of atoms.

The parallels that exist between atom optics and particle optics provide an extremely useful framework for understanding the behavior of atom optical elements. However, there is one aspect of atom optics that has no parallel in other forms of optics. This aspect is the availability, through laser cooling, of dissipative forces that can be put to use in the collimation and velocity compression of atom beams. These non-conservative forces permit circumvention of a number of restrictions that apply to both particle and light optics, and hence provide additional flexibility for atom optics.

In particle and light optics a fundamental conservation law, referred to variously as the law of sines, the Abbé sine law, or the law of Helmholtz-Lagrange, imposes limitations on the flux, or brightness, of beams in an imaging system[103]. This law can be derived from thermodynamic principles, and ultimately stems from Liouville's theorem on the conservation of phase space volume in the presence of a conservative potential. For any bundle of rays in an optical system, the law states that the product $AV\sin^2\theta$ is conserved at the object plane and at any image plane in the system. Here A is the area of the beam, θ is the divergence angle of the bundle of rays, and V represents either the local kinetic energy of the particles in the particle-optics version, or n^2, the square of the index of refraction, in the light-optics version.

The impact of this law comes when one wishes to increase the flux of a beam by focusing it down to a small spot. The law implies that to reduce the area of the beam, it is necessary to increase θ and/or V. Since there are usually external constraints on V, the practical result is that it is not possible to simultaneously brighten a beam and also collimate it (that is, reduce θ) using only conservative optical elements.

Another limitation that occurs when optics are formed with conservative potentials is the lack of freedom in altering the velocity distribution. If an ensemble of particles with a certain velocity distribution and associated mean kinetic energy passes through a conservative optical system, the velocity distribution on exiting the system is constrained by the conservation of energy to have the same mean kinetic energy spread as before. Thus particle beams cannot be monochromized by conservative optics alone. Of course conservative, dispersive elements can be used in conjunction with apertures to eliminate unwanted velocities, but there is always an

associated loss of flux with this approach.

The availability of non-conservative forces in atom optics allows the circumvention of both of these limitations. The law of sines is no longer a restriction because the conservation of phase-space volume dictated by Liouville's theorem no longer holds. Also, the restrictions on altering the velocity distribution of a beam due to energy conservation are no longer in place. Thus it is possible in principle to both collimate and brighten a beam of atoms to any degree desirable, and also to compress the velocity distribution in atom beams without any loss of flux. These unique capabilities make atom optics especially interesting from an optical point of view, and also lead to practical advantages that can in principle be exploited.

The collimation of an atom beam by laser cooling has been demonstrated in quite a few experiments. A number of geometries have been used, including transversely counter-propagating laser light in one- and two-dimensions[104], laser light focused by an axicon (conical lens)[105], laser light enhanced by a one-dimensional build-up cavity[106], and laser light in the form of a spherical standing wave[107,108]. Different cooling schemes have been utilized, including Doppler cooling[104], stimulated cooling with blue-detuned laser light[106,109,110], and polarization-gradient cooling[111]. More extensive beam brightening in conjunction with collimation has also been accomplished making use of not only laser cooling, but also magneto-optical forces. This has been done with what is referred to as an "atom funnel," where slowed atoms are sent into a two-dimensional magneto-optic trap where they are compressed and cooled radially[112,113]. Alternatively, use can be made of an extended beam-line consisting of first capturing and collimating atoms with laser cooling, then focusing them in a magneto-optic lens, and finally recollimating them with another stage of laser cooling[114]. In all these experiments, collimation was demonstrated on one of the alkali atoms Na, Rb, or Cs, one of the metastable rare gases He* or Ne*, or Cr.

Velocity compression of an atom beam, as well, has been demonstrated in a number of experiments. In the process of slowing a sodium beam with counterpropagating light, compression has been seen either with no compensation for Doppler shifts[115], compensation with a tapered magnetic field[116] or compensation by chirping of the laser frequency[117]. Also, velocity compression of a supersonic metastable argon beam has been demonstrated with two symmetrically-detuned, counterpropagating laser beams travelling along the atom beam axis, cooling the atoms in a reference frame moving with the mean velocity of the beam[118].

IV. Nanofabrication with Atom Optics.

We now turn to a discussion of some specific examples of the use of atom optics to create nanostructures on a surface. Although the discussion up to now has shown that there is a rich variety of ways to manipulate atomic beams, it is perhaps surprising that until very recently little of this knowledge base has been turned toward controlling atoms on the nanoscale to make features on a surface. One possible reason for this is the mismatch that exists between the atomic species generally studied in atom optics on the one hand, and the materials traditionally used in nanofabrication on the other. Another could be that the research methods involved in the two fields are sufficiently different that the combination is not readily accomplished. This situation

has begun to change in recent years with the introduction of a number of key developments that have brought these two fields together and stimulated significant interest in what might now be possible.

Two basic approaches to nanofabrication with atom optics have evolved from the preliminary research in this area. In one method, atoms are manipulated during direct deposition, growing nanostructures by adding atoms to the surface in a specific pattern. In the other, atoms are manipulated as they impact and expose a resist, in what is referred to as neutral atom lithography. In the next two sections, we discuss some of the results that have been obtained with these two approaches.

IV.A. Direct deposition techniques.

To date, nanofabrication by direct deposition of laser-focused atoms has been demonstrated using only one configuration—the standing wave lens array, as discussed in section III.A.6. This configuration has the advantage that it is relatively simple to set up, and it also represents one route toward fabrication of a large, coherent array of nanostructures in parallel.

The basic experimental arrangement for atom focusing in a standing wave is illustrated in Fig. 18. An effusive oven produces a beam of atoms that is first collimated by a pair of slits or apertures, and then further collimated by transverse laser cooling. This second stage of collimation is required because the angular divergence of the atom beam must typically be reduced to substantially less than a milliradian. Such a high degree of collimation is necessary because the standing-wave potential wells typically have a depth of only ~1 •eV. Considering that the longitudinal kinetic energy is generally about 100 meV, even a small transverse component of the velocity can result in a transverse kinetic energy that is larger than the potential well depth. Also, even if the transverse kinetic energy is less than the depth of the well, the ultimate spot size obtainable is very sensitive to the degree of collimation (see section IV.A.4, below).

It is worth noting that while the collimation of the atomic beam could in principle be done with very small apertures at a large separation, laser cooling has a number of advantages. For one thing, it produces the required collimation with essentially no loss of flux, in contrast with the huge flux loss associated with using small apertures. Furthermore, the incident atoms can be automatically aligned perpendicular to the standing wave if the cooling laser beam is retroreflected from the same mirror that produces the standing wave beam. Lastly, it is generally convenient to take advantage of the near-resonant laser light that is available anyway, so the method does not pose too much additional complication for the experiment.

The laser light for generating the standing wave, and also the optical collimation beam, is by necessity produced in a single-frequency, tunable source such as a dye laser, a diode laser, or a Ti:sapphire laser. The frequency must be tightly controlled because it is important to be able to tune the laser very close to the atomic resonance, especially for the laser cooling. Both the standing wave and the laser cooling beam can be obtained from the same laser source with the aid of an acousto-optic (or electro-optic) frequency shifter. Typically the laser cooling frequency

must be about one atomic linewidth (e.g., 5 MHz for Cr) below the atomic resonance, while the standing wave frequency is set several hundred MHz above the atomic resonance to minimize spontaneous emission and ensure concentration of atoms into the low intensity regions of the standing wave. The laser frequency must be locked relative to the atomic resonance to eliminate drifts during deposition, and this is accomplished either by using a saturable absorption cell or by imaging the fluorescence from a transverse probe laser beam crossing a diverging part of the atom beam onto a split photodiode[119].

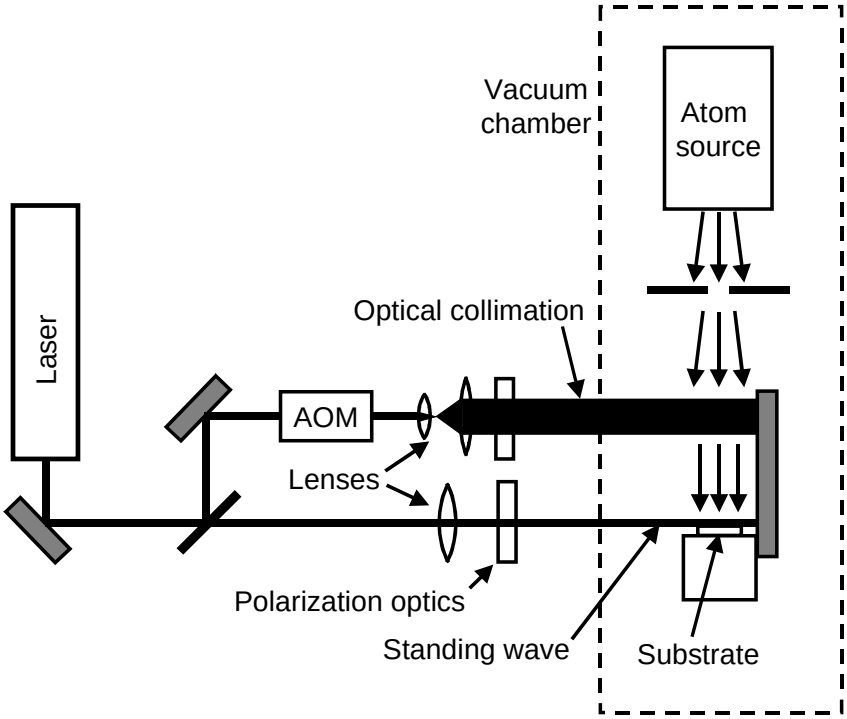

Figure 18 Generic experimental set up for atom focusing in a standing wave. Near-resonant laser light is produced in a single-frequency, tunable laser source, such as a dye laser, a diode laser, or a Ti:sapphire laser. The laser, typically tuned several hundred MHz above resonance, passes into the vacuum chamber and propagates very closely above the surface of a substrate, after which it is retroreflected to create a standing wave. A portion of the beam is split off and frequency-shifted in an acousto-optic modulator (AOM) to just below the atomic resonance to provide laser cooling for optical collimation of the atom beam. Both the standing wave and optical collimation beams are carefully shaped and polarized with appropriate optics. Within the vacuum system, an atom beam is produced in a heated oven, is precollimated by an aperture, and propagates transversely through the cooling and standing wave laser beams. As the atoms deposit onto the substrate they are focused in the nodes of the standing wave, creating an array of nanostructures.

The polarization of the laser beams must be carefully controlled. The laser cooling light is typically circularly polarized for Doppler cooling, or put in a lin $\perp$ lin configuration for polarization-gradient cooling. The latter is achieved by placing a quarter-wave plate in front of the retroreflection mirror. The standing wave polarization can in fact be either circular or linear, depending on the magnetic sublevel distribution present in the atoms as they enter the standing wave. If Doppler cooling is used in the collimation, the atoms will typically be fully optically pumped into a pure $|M| = J$ state (stretched state). Then circularly polarized light is most

appropriate, as it will have the strongest interaction with the atom. If polarization-gradient cooling is used the distribution of magnetic sublevel population tends to be spread over several levels, and linear polarization is more appropriate as it interacts more evenly with the different levels.

In mounting the sample and the standing wave mirror, it is important to ensure that their relative position is stabilized at the nanometer level so that drift or vibrations do not smear out the deposited structures. This can be done either passively, by building a rigid mount, or actively by sensing the relative position with a Fabry-Perot interferometer and correcting it with a feedback loop connected to a piezoelectric transducer. While the mirror's positional stability is critical, it is interesting to note that the laser beam's positional stability is not nearly so important. This is because the locations of the nodes of the standing wave are determined to first order only by the mirror position and the laser wavelength. The slight shifting of the nodes that results from a variation in the angle of the laser beam is only a second order effect because it depends on a cosine, which deviates from unity only quadratically for small angles.

IV.A.1. Sodium.

The first demonstration of nanofabrication by laser focusing of atoms was done with sodium[66], using an experimental set up containing the essential elements of Fig. 18. Building on earlier work in which a focused Gaussian laser beam was used as a stencil to create a millimeter-scale pattern in a deposited sodium beam[120], this work showed that a periodic nanoscale pattern could be deposited directly onto a silicon wafer. The sodium pattern was detected by observing the diffraction of a laser beam of shorter wavelength from the surface after deposition. Clear diffraction peaks were observed at the angles corresponding to the expected periodicity of the pattern, i.e., half the sodium resonance wavelength, or 294.5 nm. In subsequent work, scanning tunneling microscopy (STM) images verified the existence of the sodium features[121, 122, 123, 124]. This was done by transferring the samples to an STM operating within the vacuum system, since the sodium features reacted on exposure to air.

To achieve focusing of the sodium atoms, the laser beam, produced with a dye laser, was tuned near the $3^2S_{1/2}(F=2)$ to the $3^2P_{3/2}(F=3)$ D_2 line at 589 nm (this transition has a natural linewidth of 10 MHz and a saturation intensity of 6.3 mW/cm^2). The atom beam originated in an effusive source at 420 ºC and was collimated in the first experiments with Doppler cooling utilizing circularly polarized laser light. In subsequent work polarization-gradient cooling was also used. The standing wave, with detunings ranging from 70 MHz up to 1.7 GHz and laser powers in the few milliwatts regime, was positioned (in different experiments) at a number of distances from the substrate, ranging from directly on the surface to 200 μm above it. Optimum focusing of the sodium atoms was found with the standing wave propagating directly along the surface, such that its profile was cut in half and the maximum intensity was at the surface. For this optimum case, the detuning was 1.7 GHz, the standing wave beam waist diameter was 29 μm, and the travelling wave power was 8 mW[125].

IV.A.2. Chromium.

Shortly after the first demonstration using sodium atoms, laser control of chromium atoms was introduced, allowing the first permanent nanostructures to be made with atom optics. Chromium has the advantage that on exposure to air a very thin (~1 nm) passivating oxide layer is formed, so samples can be prepared in vacuum and then removed and inspected in air with an atomic force microscope (AFM). Using the generic set up for laser focusing in a standing wave depicted in Fig. 18, a number of demonstrations of chromium nanofabrication have been realized[67, 126, 127, 128, 129].

For nanofabrication with chromium, the laser light must have a wavelength of 425.43 nm in air (425.55 nm in vacuum), which matches the 4^7S_3 to 4^7P_4 transition. This is provided either by a dye laser operating with stilbene-3 laser dye and pumped with a UV argon-ion laser[67], or by a Ti:sapphire laser doubled in an external ring cavity[129]. The natural linewidth of this transition is 5 MHz, and the saturation intensity is 8.5 mW/cm^2. Typically, polarization-gradient cooling is used to collimate the atoms, resulting in a collimation angle as small as 0.16 mrad[111]. The atom beam is produced in an effusive cell operating at 1550-1650 °C.

Fig. 19 shows two AFM images of chromium lines obtained with laser-focused atomic deposition in a standing wave. Fig. 19a shows a three-dimensional rendering of a 1 μm-square image taken from a deposition on silicon dioxide, and Fig. 19b shows a plan view of an 8 μm-square image showing lines deposited on sapphire in a somewhat thicker deposition. These nanostructures were produced with the Gaussian standing wave (single beam power 33 mW, $1/e^2$ beam diameter 0.13 mm) propagating so that its profile was cut in half by the substrate. Fig 19a indicates how narrow the lines can be made—38 nm full width at half maximum (FWHM) in this particular case. The 8 μm-square image in Fig. 19b gives some idea of the uniformity of the lines. The peak-to-valley height of the lines, as governed by the contrast of the deposition, and also by the flux of Cr and the deposition time, is 8 nm in Fig. 19a, and 16 nm in Fig. 19b. The area covered extends for approximately 1 mm in the direction transverse to the lines, and 0.15 mm along the lines.

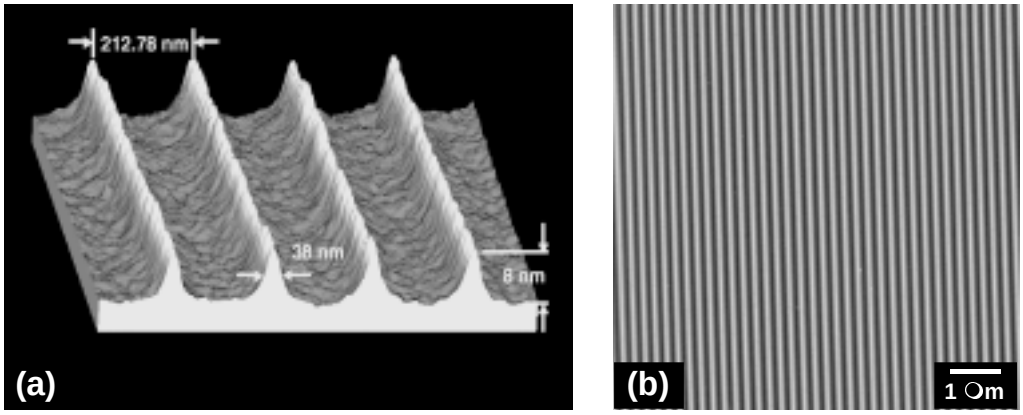

Figure 19 Atomic force microscope (AFM) images of nanostructures formed by laser-focused atomic deposition of chromium. (a) 1 •m-square image of a relatively thin deposition on SiO_2, showing 212.78 nm pitch, 38 nm linewidth (full-width at half maximum), and 8 nm peak-to-valley

distance (from J. J. McClelland *et al.*, Aust. J. Phys. **49**, 555 [1996]). (b) 8 •m-square image in plan view of a thicker deposition on sapphire, illustrating the long-range uniformity of the lines.

The samples shown in Fig. 19, and in fact all samples of laser-focused Cr nanostructures made so far, have some amount of background deposition in the regions between the lines. This background arises in part from the 16% of the atom beam that consists of isotopes other than ^{52}Cr, which do not interact with the laser. Other contributions possibly include the high-velocity tail of the longitudinal velocity distribution, wings in the transverse velocity distribution, or spherical aberration in the lens. Experimentally, the background level is found to vary somewhat with deposition conditions, with a minimum value of about 1/3 the peak-to-valley height.

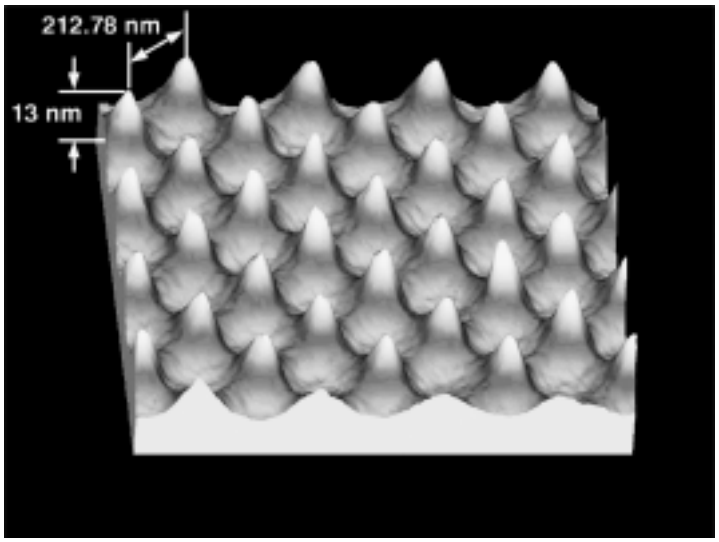

Figure 20 Atomic force microscope (AFM) image of a two-dimensional array formed by laser-focused atomic deposition of chromium using two orthogonal standing waves. Shown is a 2 •m-square image (from R. Gupta *et al.*, Appl. Phys. Lett. **67**, 1378 [1995]).

In addition to making arrays of lines, laser-focused atomic deposition of Cr has also been used to fabricate two-dimensional arrays of peaks. For example, a square array has been fabricated by superimposing a second standing wave at 90º over the first[130]. An AFM image of this pattern is shown in Fig. 20. While this orthogonal geometry is the simplest conceptually, it is necessary to be aware of the possible problems that can arise as a result of the relative temporal phase between the two standing waves. In general, the two standing waves will interfere with each other to create additional nodes, the pattern of which depends on the relative temporal phase. Since this phase is determined by the difference in path lengths taken by the two laser beams making up the two standing waves, the nodal pattern can vary if the path difference varies, as it would if influenced by acoustical vibrations. To circumvent this problem the path difference would ordinarily have to be actively stabilized. Alternatively, as described in ref. [130], the standing waves can be given orthogonal linear polarizations, with one polarization parallel to the substrate and the other perpendicular. This eliminates any interference between the standing waves and leads to a stable pattern. Another approach to the temporal phase problem is to use the interference pattern generated by three laser beams crossing at mutual angles of 120º[131]. In this case a two-dimensional pattern with hexagonal symmetry is formed,

with no dependence on relative phase. Fig. 21 shows an AFM image of a pattern formed in such a configuration.

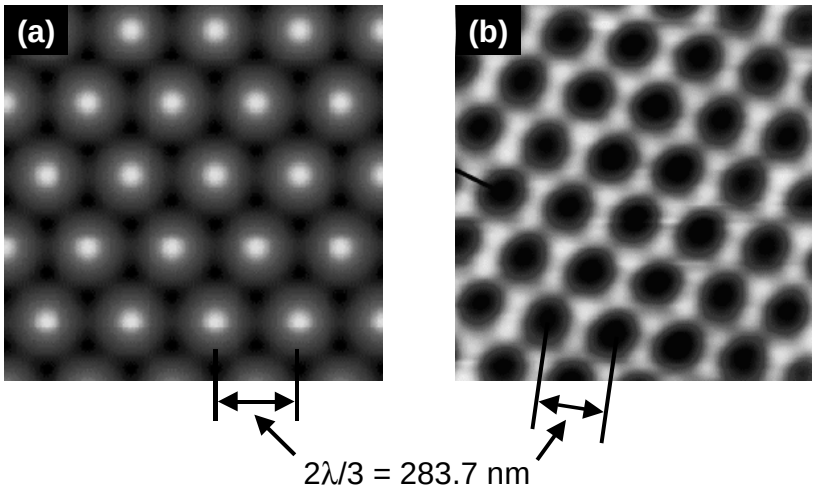

Figure 21 Atomic force microscope (AFM) images of two-dimensional arrays formed by laser-focused atomic deposition of chromium using three laser beams crossing at mutual angles of 120º. (a) Using red detuning, an array of dots is created by focusing atoms into the antinodes of the light field; (b) using blue detuning, an array of rings is formed (from U. Drodofsky *et al.*, Appl. Phys. B **65,** 755 [1997]).

In the one- and two-dimensional patterns shown in Figs. 19 and 20, the periodicity is fixed at half the laser wavelength, or 212.78 nm. Recently, it has been demonstrated with chromium that the line spacing can be reduced to $\lambda/8$, or 53.2 nm[132]. This is accomplished by changing the polarization in the standing wave to the lin $\perp$ lin configuration, in which two travelling waves with orthogonal linear polarizations counterpropagate. With this polarization configuration, the optical potential generated by the standing wave can no longer be considered a simple sine wave. Instead, the complex interactions of all the magnetic sublevels in the Cr ground state with the light polarization that varies across the wavelength must be considered. Taking proper account of these interactions, one finds that the motion of the atoms is governed by an array of seven adiabatic potentials, some of which have minima at even multiples of $\lambda/8$, and some of which have minima at odd multiples of $\lambda/8$. The result is an array of lines with four times the periodicity of the lines produced with ordinary polarization. An example of this type of pattern is seen in the AFM image shown Fig. 22, which shows an array of lines with 53.2 nm spacing. We note that in this type of deposition, the background level tends to be higher, with the modulation depth of the Cr surface reaching only about 50% of the average film thickness.

In discussing nanofabrication by laser focusing of chromium, it is worth mentioning a number of extensions that have been realized making use of the Cr lines to construct nanostructures out of more diverse materials. One example of this is the use of the Cr lines as a template for replica molding[133]. In this process, a mold of liquid prepolymer poly(dimethylsiloxane) (PDMS) is cast against the original Cr lines. The resulting elastomeric mold is peeled from the substrate and used as a mold for photochemically-curable polyurethane. The result is a rigid replica of the original lines with excellent fidelity. An AFM image of such a

mold is shown in Fig. 23.

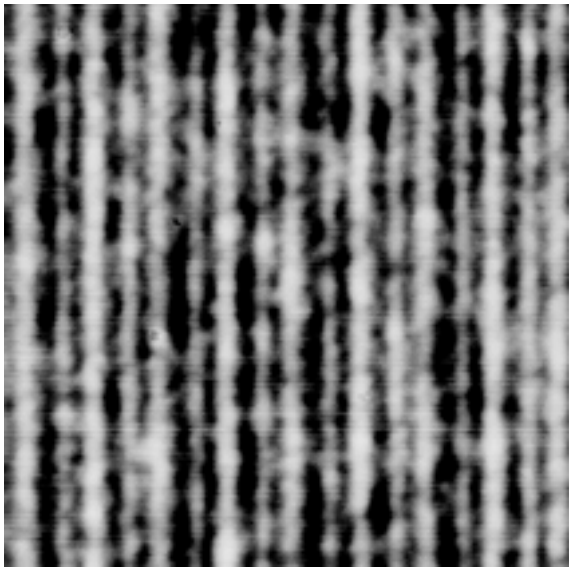

Figure 22 Atomic force microscope (AFM) image of chromium lines with λ/8 spacing, produced by focusing atoms in a lin ⊥ lin standing wave. The average pitch is 53.2 nm (from R. Gupta et al., Phys. Rev. Lett. **76**, 4689 [1996]).

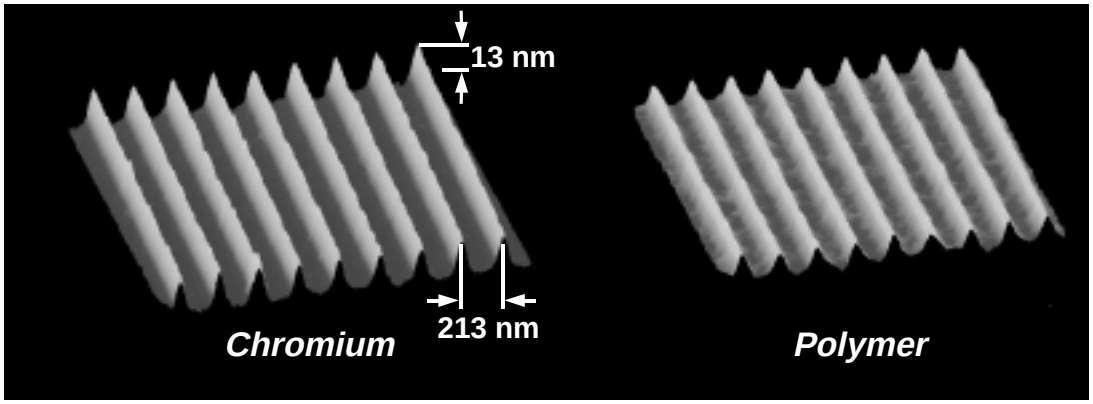

Figure 23 Replication of chromium features made by laser-focused atomic deposition. Shown are atomic force microscope (AFM) images of the original chromium lines and a polyurethane cast of them made by forming an intermediate mold of poly(dimethylsiloxane) (from Y. Xia et al., Adv. Mater. **9**, 147 [1997]).

Another example is the fabrication of nanoscale magnetic materials. In a demonstration of this, Fe was evaporated at a grazing angle of 10º onto the sides of the Cr lines, resulting in an array of magnetic lines with width less than ~100 nm and length of about 150 μm[134]. Fig. 24 shows an image of such an array of lines, taken with a scanning electron microscope with polarization analysis (SEMPA)[135]. In this image, magnetization in one direction along the

lines shows up as white, and magnetization in the other directions shows up as black, with unmagnetized Cr showing up as gray between the lines. Clear black and white domains are seen in the magnetic nanolines, indicating that shape anisotropy has forced the magnetization to be oriented only along the long axes of the lines, in one direction or the other.

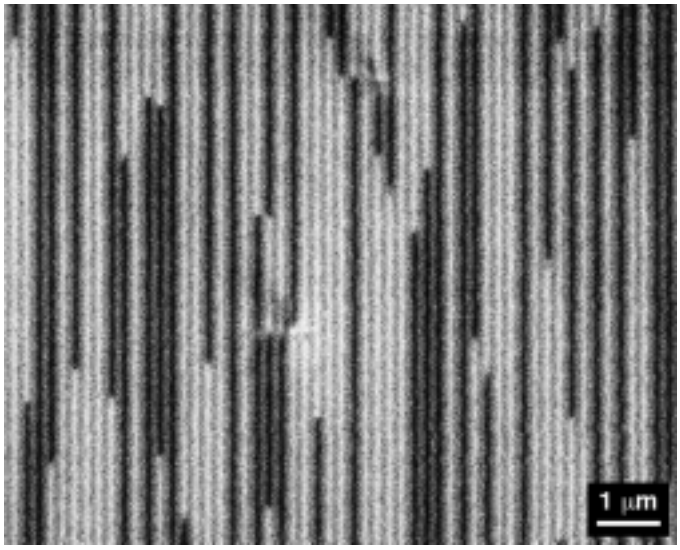

Figure 24 Magnetic nanowires formed by evaporation of iron at grazing incidence onto lines made by laser-focused atomic deposition of chromium. The image is taken with scanning electron microscopy with polarization analysis (SEMPA), which is sensitive to the magnetization of the surface of the specimen. In this image black indicates magnetization in one direction along the lines and white indicates the other. The gray regions between the lines indicate the lack of magnetization of the chromium substrate exposed between the iron wires (from J. J. McClelland *et al.*, SPIE Proceedings **2995**, 90 [1997]).

In addition to replicating from the Cr lines and depositing on them, it is also possible to use reactive-ion etching to modify their shape and/or transfer the pattern to the substrate. A recent demonstration of this has shown that a number of distinct forms can be made[136]. The various forms are created as a result of the interplay between slow sputtering of the Cr lines and rapid etching of the Si substrate. Initially, the Cr film is sputtered uniformly until the regions between the lines are cleared of Cr. Then reactive-ion etching takes over on the substrate, forming rapidly-deepening trenches while the Cr lines are gradually thinned and narrowed by sputtering. After a fixed etching time, the result will either be narrow trenches in the silicon substrate, an array of well-separated Cr ribbons on silicon pedestals, or an array of narrow (~70 nm) Cr wires (see Fig. 25). Which form occurs depends on the initial contrast of the Cr deposition: lower contrast leads to narrow trenches, and higher contrast leads to increasingly narrow Cr lines and deeper trenches.

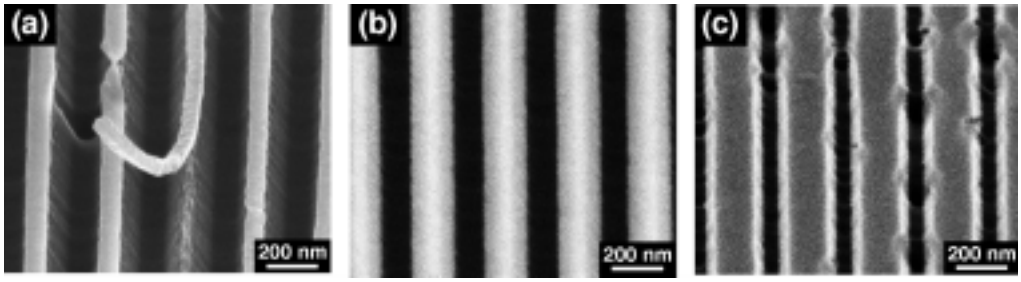

Figure 25 Scanning electron microscope (SEM) images showing reactive-ion etching of chromium nanostructures formed by laser-focused atomic deposition. (a) Region of relatively high contrast in the original deposition, showing narrow (68 nm wide) chromium wires atop sharp silicon ridges; (b) region of intermediate original contrast, showing the formation of well-separated chromium ribbons; (c) region of low original contrast, showing narrow trenches cut into the silicon (from J. J. McClelland *et al.,* Appl. Phys. B [in press]).

IV.A.3. Aluminum.

Besides sodium and chromium, the only other element that has been successfully focused and deposited on the nanoscale using atom optics is aluminum[68]. As with the other two elements, the configuration employed was the standing-wave lens array, and a set up similar to what is shown in Fig. 18 was employed.

While good reasons exist for making nanostructures from aluminum, such as its superconducting properties and its use as an interconnect material in integrated circuits, it also poses some special challenges for laser-focused atomic deposition. The optical transition in the aluminum atom most appropriate for optical manipulation is between the $3^2P_{3/2}(F=4)$ ground-state level and the $3^2D_{5/2}(F=5)$ level. This transition has a wavelength of 309.4 nm, a natural linewidth of 13 MHz, and a saturation intensity of 57mW/cm^2 [137]. Since this transition is in the ultraviolet, the simplest sources of tunable laser light are not useful. Nevertheless, a dye laser can be frequency-doubled to provide the necessary light for both collimating and focusing the atoms. In the work described in ref. [68], a single-frequency ring-dye laser operating at 618 nm was doubled in an astigmatically-compensated external ring build-up cavity using a $LiIO_3$ nonlinear crystal. Up to 40 mW of tunable laser light at 309.4 was obtained, which was sufficient for both the transverse cooling and laser-focusing of the atoms.

Unlike sodium and chromium, where essentially all the atoms are in (or can be put into) a single ground state that interacts with the laser, aluminum has its ground state population spread out over a number of levels that are thermally populated. Not only are the other hyperfine levels of the $3^2P_{3/2}$ state statistically populated, but so also are the levels of the $3^2P_{1/2}$ state, which lies 14 meV below the $3^2P_{3/2}$ state. As a result, only 25% of the atoms in a thermally-produced beam are accessible to a single laser frequency (in principle, of course, additional lasers could be used to optically pump more atoms into the resonant level if desired).

Despite these experimental complications, clear nanostructures of aluminum have been fabricated. For the experiments described in ref. [68], the standing wave laser beam had a single-beam power of 16.7 mW, a waist radius of 0.11 mm, and was linearly polarized. The laser

cooling was performed with 7.6 mW of single-beam laser power in a lin ⊥ lin configuration for polarization-gradient cooling. The detuning was 210 MHz below resonance for the standing wave, and 10 MHz below resonance for the laser cooling.

Like chromium, the aluminum nanostructures are passivated by exposure to air, and can be removed from vacuum for examination with an AFM. Fig. 26 shows an AFM image of the aluminum lines, where the expected 155 nm periodicity is clearly visible. These lines have an average height of 3 nm, a FWHM of ~80 nm, and an average background level of ~30 nm.

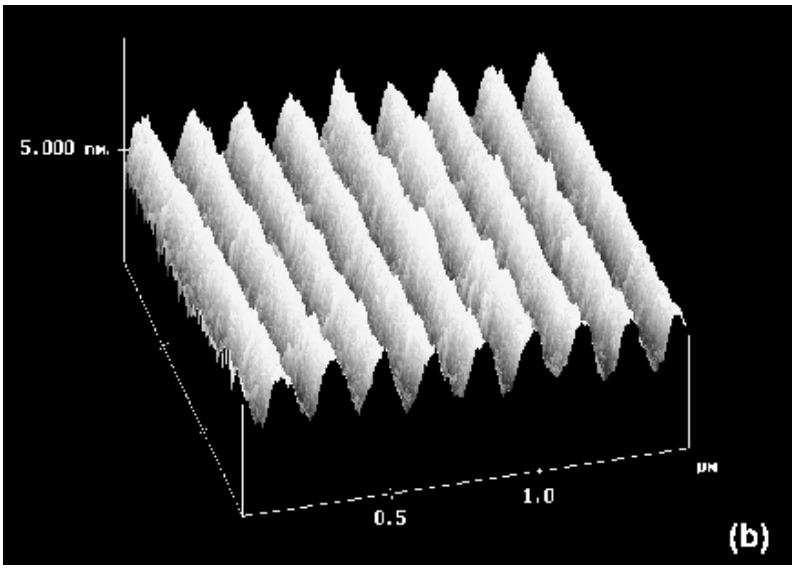

Figure 26 Atomic force microscope (AFM) image of aluminum lines formed by laser-focused atomic deposition. These lines have a periodicity of 155 nm, a full-width at half maximum (FWHM) of ~80 nm, and a peak-to-valley height of 3 nm (from McGowan *et al.*, Opt. Lett. **20**, 2535 [1995]).

IV.A.4. Modeling of a standing-wave lens.

Along with the experimental investigations of focusing atoms in a standing-wave lens, several calculational tools for analyzing the lens have also been developed. These tools cover three levels of increasing complexity, and these can be put to use according to the degree of detailed information desired.

The most basic approach is to consider the motion of the atoms through the standing wave as governed by the paraxial approximation to the trajectory equation (see section III.A.10, eq. (15), and ref. [74]). From this equation the first order focusing properties of the lens can be obtained, from which gross estimates of the behavior can be derived. Defining z as the coordinate along the direction in which the atoms predominantly travel (i. e., perpendicular to the surface), and x as transverse to z, along the laser propagation direction, the paraxial equation becomes[74]

$$\frac{d^2x}{dz^2} + q^2 g(z) x = 0, \qquad (18)$$

where

$$q^2 = k^2 \frac{\hbar\Delta}{2E_0} \frac{I_0}{I_s} \frac{\Gamma^2}{\Gamma^2 + 4\Delta^2}, \qquad (19)$$

in which $k=2\pi/\lambda$ is the laser wavenumber, Δ is the detuning, E_0 is the kinetic energy of the atoms, I_0 is the peak intensity of the standing wave, I_s is the saturation intensity of the atom, and Γ is the atomic transition probability. The function $g(z)$ describes the z-dependence of the laser intensity, i.e., its profile as encountered by the atoms on the approach to the surface.

While $g(z)$ could in principle take on a range of forms, in practice it has almost exclusively been very close to a Gaussian profile with $1/e^2$ width σ, that is, $g(z) = \exp(-2z^2/\sigma^2)$. With this profile the focal properties of the lens can be derived in either the thin lens condition, when the atoms focus well beyond the standing wave, or the thick lens condition, when the atoms focus within the standing wave. In the thin lens case the focal length is given by[74]

$$f = \left(\frac{2}{\pi}\right)^{1/2} \frac{1}{\sigma q^2}. \qquad (20)$$

Considering eq. (20) together with eq. (19) for q^2, we see that the focal length is inversely proportional to the laser intensity, and directly proportional to the kinetic energy of the atoms, or equivalently, the square of their velocity. These simple facts provide useful insight into the basic behavior of the lens.

The thick, immersion lens limit, where the atoms can focus within the lens, is the most appropriate for the experimental situation when the standing wave propagates as close as possible to the substrate surface. In this case it is not sufficient to consider only the focal length of the lens; one must also take into account a principle plane whose position relative to the center of the Gaussian beam envelope varies with lens strength. While an analytic solution of the paraxial equation in this limit, yielding the principal plane location and focal length, is not possible, it is nevertheless feasible to carry out a simple numerical integration with scalable parameters that gives the behavior of the lens. This has been done in ref [74], where more details can be found of the exact behavior.

To gain some insight in the general behavior of the lens in the thick, immersion regime, it is instructive to consider the constant intensity limit, that is, the case when $g(z)=1$. The trajectories are particularly simple in this case, as the solution to eq. (18) is a linear combination of sin qz and cos qz. From this solution the principal plane location z_p can be derived to be

$$z_p = \frac{\pi - 2}{2q}, \qquad (21)$$

and the focal length takes on the simple form

$$f = q^{-1}. \qquad (22)$$

Interestingly, we note that the focal length in this regime is inversely proportional only to the first power of the velocity, instead of to the square of the velocity as it is in the thin lens case.

Given the focal length of the lens, some basic properties of the focusing can be estimated. For instance, the diffraction limit to the deposited linewidth can be estimated using eq. (11). Also, the linewidth limitation d due to an atom beam collimation angle θ can be estimated by the formula $d = f\,\theta$, which follows from the Gaussian lens law (eq. [9]) in the limit of large object distance s_1[74].

While the paraxial equation is very useful for determining the general operating parameters of a standing-wave lens, and also seeing the true lens-like behavior in terms of focal lengths and principal planes, more is needed if a realistic estimate of deposition linewidths is to be approached. This is especially true if there are significant velocity and angular spreads in the incident beam of atoms. The next level of analysis that has proven useful for analyzing focusing of atoms in a standing wave is a classical trajectory approach that numerically solves the exact trajectory equations (eqs. [16] and [17]) for a large number of trajectories of different starting conditions. Starting with an assumption (or measurement) of the velocity and angle distributions in the incident atom beam, the calculated trajectories can be used to derive a flux distribution at any point along the focusing by adding up the contributions from the various trajectories. The result is a calculation of an atom spatial distribution that provides the necessary information on the focusing of the lens.

Two examples of such a calculation are shown in Fig. 27. In Fig. 27a, the calculation is done assuming a monochromatic, parallel beam of Cr atoms, and the laser beam parameters are chosen for optimum focusing. The resulting flux distribution at the focal plane is surprisingly narrow, considering that the paraxial condition does not hold for many of the trajectories. The small width and pedestal of the central peak that are visible are in fact due to trajectories that do not quite make it to the focus because they enter the lens too far from the axis. In the language of lens aberrations, these features can be attributed to spherical aberration. This calculation shows how important (or unimportant) deviations from the paraxial equation are in a given lensing situation, and hence gives information on their contribution to the deposition linewidth.

Fig. 27b shows a calculation for incident atom beam conditions that are closer to what is often found in an experiment—a thermal velocity spread, and an angular spread as might come out of polarization-gradient transverse laser cooling. We see that in this case the trajectories do not all converge to a well-defined focus, but are in fact “channeled” into a small region (see section III.A.11). This channelling now becomes the object of attention in the calculation, since it determines what sort of linewidth can be expected. Clearly the paraxial approximation trajectories and the lens focal properties derived from them are less relevant in this case. The

type of ray-tracing calculations displayed in Fig. 27, though, can be very helpful in understanding the behavior of realistic attempts to focus atoms in a standing wave, and can provide an invaluable guide for adjusting laser beam parameters.

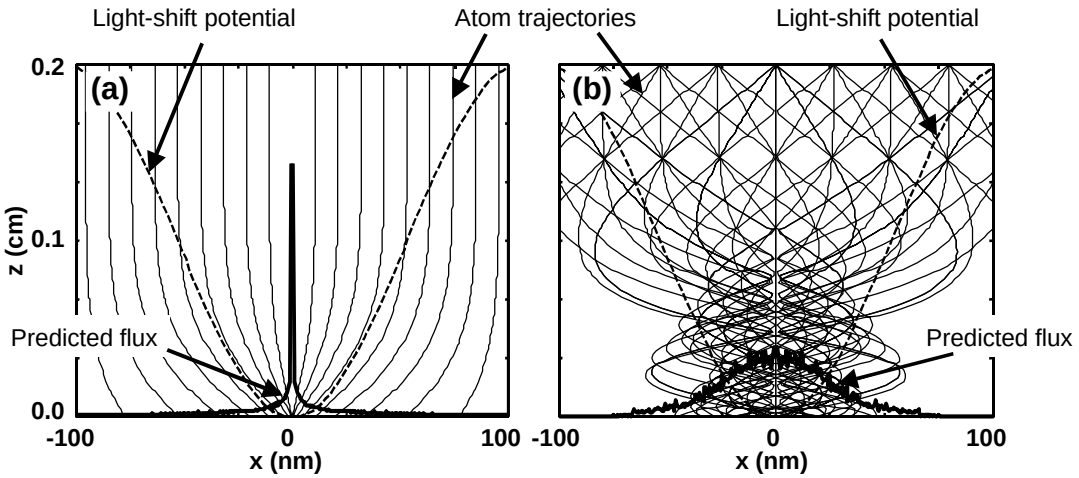

Figure 27 Calculations of atomic trajectories during focusing induced by the light-shift potential in a laser standing wave. Shown is a singe period of ths standing wave. The light is assumed to have a Gaussian profile with maximum at the surface ($z = 0$). (a) Calculation for monochromatic atoms with zero angular divergence. Note predicted flux at the surface is extremely narrow (of order 1 nm). (b) Calculation for atoms with a thermal velocity spread and angular spread corresponding to typical collimation by laser cooling. Note the atoms are "channeled," rather than focused, yet still maintain a relatively well-concentrated flux distribution at the surface. The laser intensity and detuning in (a) are chosen so that the lens is "in focus" in the paraxial approximation; for (b) the intensity is many times higher to achieve effective channeling.

While classical ray tracing calculations provide good insight into the behavior of a standing-wave lens, and are relatively easy to implement, they leave out certain details that could prove important in some situations. Two potentially significant aspects of the laser-atom interaction that are neglected are (1) the wave nature of the atomic motion, and (2) the true light-shift potential in terms of the dressed atomic energy levels, in particular the subtle effects that arise from spontaneous emission and the magnetic sublevels of the atom. To approximate the effects of the wave nature of the atomic motion, use can be made of the powerful analogies that exist between light optics and particle optics. These allow one to simply infer many diffraction phenomena, for example the diffraction limit of a focal spot that is estimated with eq. (11). However, it must be recognized that in some cases, for example in the channelling regime, optical diffraction analogies do not exist and a more complete theory must be employed. The same holds true when the true light-shift potentials must be taken into account, for instance when multiple light-shifted potentials play a role, or spontaneous emission makes the potential no longer conservative.

In such situations, resort can be made to fully quantum calculations that treat all possible interactions exactly and quantize both the atomic internal and external degrees of freedom. While analogies between the atomic motion and common optical phenomena are lost with this approach, what is gained is the possibility of an exact prediction of what sort of atomic

distribution is expected during the deposition. Such calculations have been performed to analyze the quantized motion of atoms in a standing wave[28,138], in laser cooling[36,139] and in the deposition of a $\lambda/8$-period pattern in Cr as discussed in section IV.A.2 above[132].

IV.B. Neutral atom lithography.

As discussed in the previous section, a number of demonstrations of nanofabrication with atom optics have been carried out using the direct deposition of atoms. An alternative approach to this is to employ neutral atom lithography. In this process a resist-coated surface is exposed to a patterned neutral atom beam, and then etched with an agent that differentially penetrates the damaged resist and transfers the pattern to the surface. Thus neutral atoms replace the conventional exposure agents—photons, electrons, or ions—in a process akin to conventional lithography. The advantages gained by using neutral atoms lie in the new opportunities afforded by atom optics, including the possibility of exposing large areas with nanometer-scale resolution, the reduction of substrate damage, and the elimination of diffraction and space charge as resolution limitations.

Because neutral atom beams typically have very small kinetic energies, being thermally produced, exposure of a resist requires going beyond the simple transfer of kinetic energy that is the main exposure mechanism with electron and ion beam lithography. Two separate processes have been identified as being useful for pattern transfer in this respect. One process involves chemically altering the surface, and the other involves transferring internal energy from the atom to the surface.

Exposing a resist by chemical means can be achieved by using a reactive species of neutral atom. The alkali atoms are ideal for this purpose because they are easily manipulated by lasers and they are also quite chemically active. Li, Na, K, Rb and Cs have all been the subject of extensive studies of atom manipulation, and so are natural candidates for neutral atom lithography.

Internal energy transfer is readily done with metastable rare gas atoms. These atoms, which are all susceptible to laser manipulation via optical transitions from the metastable state to a higher-lying state, carry a significant amount of energy, ranging from 20 eV for He* to 10 eV for Kr*. This energy cannot escape from the atom unless a perturbation occurs, such as when contact with a surface is made. Thus the metastable atoms can travel through a vacuum system and only lose their energy when they strike the surface of the resist, causing damage, or exposure, in the process.

One special property of the metastable rare gases Ne*, Ar* and Kr* that makes them particularly interesting from an atom optics point of view is their ability to be quenched by laser light—that is, to be radiatively transferred out of the metastable state to the ground state. This opens the possibility of patterning the atom beam by selectively quenching regions of the beam instead of modifying the atom trajectories. For example, a laser standing wave of sufficient intensity can be used to impose on an atomic beam a pattern of lines with width as small as $\lambda/25$, as atoms are quenched everywhere except in narrow regions near the nodes[140].

Quenching in a metastable atom is achieved by tuning a laser from the metastable state to a higher-lying state that has a large transition probability to the ground state. This opens a pathway to the otherwise inaccessible ground state, quickly removing the energy content of the atom and eliminating its resist-damaging capability. Quenching transitions for the metastable species Ne*, Ar* and Kr* generally lie in the visible to near-infrared region, so they can be readily accessed with available lasers.

Whether chemical exposure or energy deposition is used to transfer the pattern to the resist, care must be used in selection of a suitable resist material. Conventional resist materials, such as PMMA (polymethylmethacrylate), are generally not appropriate for neutral atom lithography because they are too thick—the damage mechanisms involved with neutral atoms are restricted to only the very surface of the resist material, so insufficient exposure would occur. A class of chemicals that do work well as resists for atom lithography are those that form self-assembled monolayers (SAMs) on a surface. Examples of these include alkanethiolates, which self-assemble on gold surfaces, and siloxanes which form on silicon substrates. With SAMs, the monomolecular layer that forms is tightly bound to the surface, and generally protects it from etching. When damaged, however, the films allow etchants to penetrate, providing the mechanism for pattern transfer.

In addition to SAMs, another resist system has been shown to be effective. This involves using what is referred to as "contamination lithography." Here, an unprotected surface is placed in a vacuum system with some background pressure of hydrocarbons and/or silicone pump oil. During exposure to the atoms, the background material that has accumulated on the surface is polymerized and becomes hardened. This turns out to be an excellent etch mask, and some very interesting features have been fabricated using this process.

Demonstrations of neutral atom lithography have until very recently been restricted to showing that the basic process works, without particular attention to combining it with atom optics. The first demonstration was done using Ar* atoms to expose a SAM of dodecanethiolate (DDT) on a gold film evaporated onto a silicon substrate[141]. In this work, Ar* was produced in a flowing-afterglow DC discharge source, collimated, and directed at the SAM-covered substrate through a mask made from a copper grid with 5 μm-wide lines. After exposure to a dose of about 10^{16} metastable atoms per square centimeter, the substrate was removed from the vacuum system and etched in a ferricyanide solution. On examination by eye, and in a scanning electron microscope (SEM), a clear shadow of the grid was seen etched into the gold (see Fig. 28). To verify that the exposure of the SAMs was caused only by the metastable atoms, and not by possible photons or fast neutrals in the beam, a control exposure was carried out with the Ar* atoms quenched by a laser tuned to the $4s\ ^3P_2 \rightarrow 4p\ ^1D_2$ transition at 764 nm. Significantly less damage was observed with the metastables quenched, indicating that the effect was real.

Building on this initial demonstration, a number of further experiments have yielded significant results. Under similar experimental conditions in two separate laboratories, He* has also been shown to expose DDT SAMs, and with somewhat higher efficiency[142,143]. In addition, metastable atoms have been found to be very effective at producing contamination resist. This has been demonstrated using Ar* to expose Si, SiO_2, or gold through a SiN membrane mask. After wet etching, clear features as small as 50 nm were seen[144]. Further refinement of this process has been achieved by switching the exposing atom to Ne*, the

substrate to GaAs, and using chemically-assisted ion-beam etching[145]. The result, an example of which is shown in Fig. 29, is a remarkably well formed pattern.

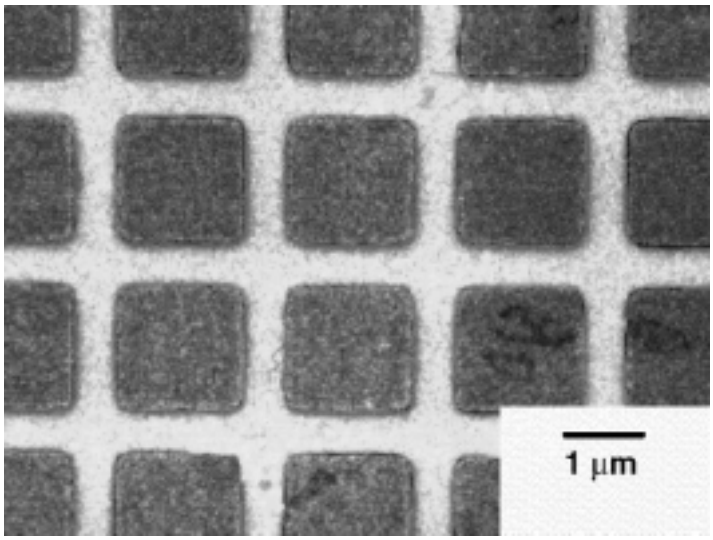

Figure 28 Neutral atom lithography with metastable argon atoms. A gold film evaporated onto a silicon substrate is coated with a dodecanetiolate self-assembled monolayer (SAM). A beam of metastable argon atoms, shadowed by a mesh, strikes the surface. On placement in a ferricyanide solution, the regions of the SAM damaged by metastable argon impact allow the underlying gold to be etched. Shown is a scanning electron microscope image of the grid shadow etched into the gold surface (from K. K. Berggren *et al.,* Science **269**, 1255 [1995]).

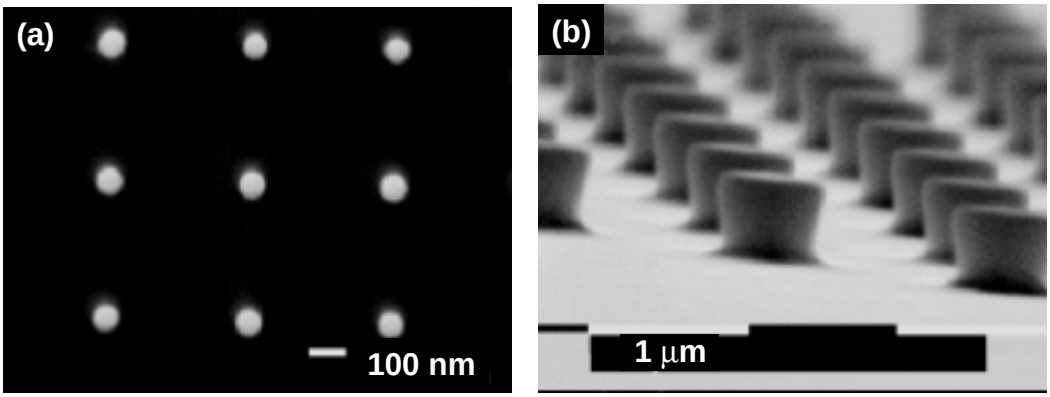

Figure 29 Contamination lithography with metastable neon atoms. A beam of metastable neon atoms passes through a mask and strikes a surface. Surface contaminants, such as hydrocarbons and/or silicone diffusion pump oil, form a hard resist when impacted by a metastable atoms. On etching, the areas of the substrate not impacted by metastable atoms are removed. Shown are scanning electron microscope (SEM) images of (a) 50 nm pillars and (b) 500 nm square posts, formed in GaAs by exposure through a SiN mask, followed by chemically-assisted ion beam etching (from S. J. Rehse *et al.,* Appl. Phys. Lett. **71**, 1427 [1997]).

Atom lithography through chemical damage with alkali atoms has also seen demonstration via a number of routes. Alkanethiolate SAMs on gold have successfully been used to transfer a pattern formed in a Cs atom beam. Fig. 30 shows the result of exposing a

SAM of nonanethiolate to thermal Cs atoms passing though a grid, followed by etching in ferricyanide solution[146]. Maximal contrast was achieved in this work with a dose of only $1.6–2.5 \times 10^{15}$ Cs atoms/cm^2 (3–5 Cs atoms per SAM molecule). Similar results were found using a SiN membrane mask to create 50 nm structures[147], and also using an octylsiloxane SAM on SiO_2 instead of the alkanethiolate SAM on gold resist system[148].

Very recently, the work with Cs atoms has been extended to include the first atom-optical implementation of neutral atom lithography[149]. To demonstrate an atom-optical process, Cs atoms were focused using an optical standing wave in an experimental set up similar to what has been done with direct deposition (see section IV.A). Using a nonanethiolate SAM on gold, and etching with ferricyanide after exposure, an array of nanoscale lines was formed in the gold. Fig. 31 contains an AFM image of this pattern, which clearly shows the expected periodicity of half the Cs resonance wavelength, or 426 nm.

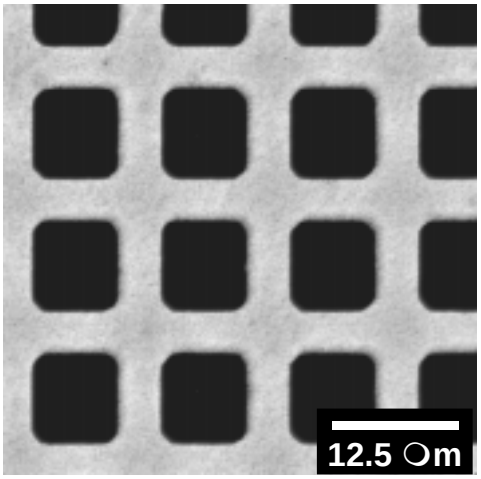

Figure 30 Neutral atom lithography with cesium atoms. A beam of cesium atoms passes through a mesh and strikes a gold film covered with a nonanethiolate self-assembled monolayer. On etching in ferricyanide solution the gold film is removed in the regions exposed to the cesium atoms. Shown is a scanning electron microscope (SEM) image of the etched gold film (from M. Kreis et al., Appl. Phys. B **63**, 649 [1996]).

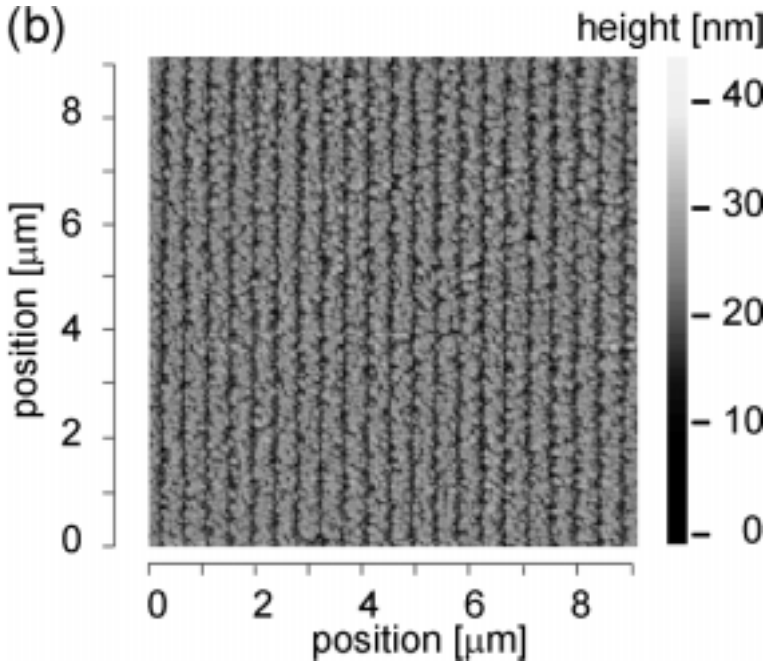

Figure 31 Nanoscale neutral atom lithography with cesium atoms. In an experimental set up similar to that shown in Figure 18, cesium atoms are focused in a standing wave lens array as they are incident on a nonanethiolate-coated gold film. On etching in ferricyanide solution, the nanoscale pattern of focused atoms is transferred to the gold film (from F. Lison *et al.* Appl. Phys. B **65**, 419 [1997]).

V. Future Prospects.

As can be seen by the discussion in the previous sections, the field of nanofabrication via atom optics is just beginning to emerge as an area of study leading to new ways to fabricate structures on the nanoscale. A strong foundation has been laid by a wealth of research on fundamental atom optics, covering many different ways to manipulate free, neutral atoms. However, this research is only just now starting to be applied to the control of atomic motion during the approach toward a surface, with the goal of creating nanostructures. Based on the initial results, it seems that a number of possibilities have been opened; it remains now to explore further to find out what extensions and limitations will be forthcoming. Though it is difficult to predict the evolution of any field of research, a few areas in which it appears that progress can be made do present themselves.

V.A. Resolution limits.

One of the most fundamental issues that needs to be investigated is the ultimate practical resolution that can be expected with atom-optical techniques. In discussing resolution, the factors that play a role can be divided into two main categories—those that arise from the atom optics (including source properties), and those that arise from the atom interaction with the

surface.

From the atom optical perspective, resolution can be addressed by analyzing the aberrations and spot size limitations expected for a variety of atom lenses. These considerations show that atom optical elements are in fact capable of extremely high resolution, but the attainment of this is hampered by the optical quality of atom sources. In all the lensing scenarios discussed in section III.A, chromatic aberration and source collimation (or effective source brightness) play a major role in determining the ultimate spot size. Yet atom sources are typically very far from the ideal in this respect, having broad, thermal velocity distributions and wide angular spreads. Improvements in atom sources, ranging all the way from the use of laser manipulation to brighten and monochromize a beam, to the production of a practical Bose-Einstein condensate, will have a significant impact on the attainable focal spot size.

Even if atom optical methods could focus atoms into an infinitely narrow spot, however, the behavior of the atoms during and after surface impact could play a crucial role in determining the size of the resulting feature. This is true in either the direct deposition or the atom lithography case. In direct deposition, surface diffusion and grain growth could play significant roles in determining where the deposited atoms finally come to equilibrium. This could seriously impact, or even completely determine, the size of the structures deposited, regardless of the resolution of the atom optical focusing. To complicate matters, these effects would be dependent on the particular atom-substrate system under investigation, and also the contamination level. In atom lithography, where resists are used, the energy-deposition or chemical process that exposes the resist will have a certain spatial range over which it has an effect. This spatial range is presently unknown, and could conceivably be very small. On the other hand it could be larger than the focal spot created by the atom focusing, becoming the limitation on the resolution of the process.

V.B. More complex patterns.

Another avenue of future investigation with potentially fruitful outcome concerns the extension of the basic atom optical processes demonstrated to date to encompass the fabrication of more complex patterns. This could proceed on a number of levels. Utilizing the basic standing wave concept, with which large arrays of lines and dots have been made, a fairly straightforward extension would be to make an array of dots and then scan the substrate during deposition. Scanning within the range of a unit cell of the array, for example with a piezoelectrically actuated stage, the atom lenses could be used like an array of “atom pens,” writing many identical complex patterns with a periodicity governed by the standing wave.

Going beyond this, the standing wave field could be generalized into a more complex interference pattern. Using a number of laser beams incident from a range of angles, one could conceive of creating a very complex pattern. The challenge here would be to start with a given, desired pattern and find how many laser beams incident from which angles and with what relative phase will be required to generated this pattern. This would have to be done working within the laws of diffraction, and also with the limitation that the laser wavelength is the same for all beams because of the atomic resonance requirement. While it appears that a broad range of patterns could be generated in this way, it also seems that limitations will be encountered. It

remains for future research to find out just what can be accomplished.

Another approach is to work on development of an atom optical projection system. Here, an atom beam patterned by a mask is imaged by an atom optical system with some demagnification, creating an arbitrary pattern on a surface with potentially nanoscale feature size. With this approach, advantage is taken of the true imaging characteristics of atom optical lenses, which in principle can be very good because the diffraction limit can be very small. Along with these good imaging characteristics, however, come the technical challenges of atomic source optical quality, lens aberrations, field of view, off-axis aberrations, etc., which become much more critical in a true imaging situation.

V.C. Other atoms.

So far, nanofabrication with atom optics has been demonstrated with few atomic species and materials. Direct deposition has been implemented with sodium, chromium and aluminum, and atom lithography has been shown to be effective with metastable rare gases and alkalis on self-assembled monolayer resists. To fully realize the potential of this technique, it is worth considering the issues that govern what other atoms could be used.

The first consideration that must be taken into account in evaluating the feasibility of manipulating a particular atom is the possibility of making a monoatomic beam of sufficient flux. Any element will evaporate if heated to a high enough temperature, but making atomic beams can be tricky, sometimes involving complex high-temperature materials issues. Furthermore, some atom beams tend to have a large fraction of dimers or other molecular forms, which can add a background level if not separated out somehow (e.g., by laser deflection of the desired atoms). There is, however, a fairly well established technology of making a wide range of beams, so in many cases methods have already been established[150].

The next consideration depends on what sort of atom optics will be implemented. For purely magnetic focusing, any atom with a ground state magnetic dipole moment is in principle manipulable. This encompasses quite a few atoms, since any atom with an unfilled shell will in general have some angular momentum and hence a magnetic dipole moment. If, however, the additional capability of laser-based atom optics is desirable, the range of possible atoms is restricted to those with appropriate optical transitions. In fact, many atoms do have the right sort of transition; the issue becomes whether a sufficiently powerful laser source exists that can be tuned near enough to the resonance to have a strong enough effect. Many atoms have their strongest transitions in the deep ultraviolet, making this requirement technologically more challenging. A further complication arises if an atom has a number of naturally occurring isotopes. These will typically have shifted resonance frequencies due to hyperfine structure and isotope shifts, causing them to interact differently with the laser light and possibly resulting in unwanted background effects.

If the laser-based atom optics to be used relies on creating an excited-state population that persists for more than a short time, such as if laser cooling is to be implemented, an even further restriction is imposed. Now there must be no population sinks—that is, intermediate metastable levels into which atomic population can decay from the excited state, remaining there without

interacting with the laser. This last requirement, being quite restrictive, is the major reason why the study of atom manipulation has so far been restricted to only a handful of atoms. It should be noted, however, that in many cases where population sinks exist, additional laser light can be introduced to repump the atoms back into the ground state, allowing them to be interact with the manipulating laser again.

Given these requirements, it appears that the generalization of laser-based atom optics to other atoms is not trivial. Nevertheless, there are many atoms in the periodic table, and each of them has a very large number of optical transitions. The feasibility of manipulating any particular atom cannot be dismissed without carefully considering all the possible optical transitions to see if some combination of laser frequencies and transitions, perhaps involving a metastable state, could be used. An invaluable resource for such a study is a compilation of atomic energy levels and transition probabilities, such as is found in ref. [151].

V.D. Applications.

Since nanofabrication with atom optics is in the very early stages of development, it is perhaps too early to discuss specific applications for which it will be useful. Nevertheless, it is already possible to see generic directions in which the process has natural capabilities, and also a few direct applications for the technology as it exist today.

One of the clear advantages that laser-focused atomic deposition has over most other nanofabrication techniques is the inherently resist-free nature of the process. By directly depositing atoms on a surface, it is possible to avoid many of the disadvantages of using a resist, such as the extra steps involved in applying and stripping the resist and the possibility of contamination associated with these steps. Thus in contamination-sensitive nanofabrication processes, it could be very useful to develop atom-optical alternatives to current methods.

Another general area in which atom optics has an inherent advantage is the fabrication of any structure that requires a large array of identical substructures. This type of application can take advantage of the standing wave lens array and its natural periodicity to conveniently pattern a large area in parallel. A good example of such an application is the fabrication of photonic materials. Here, arrays are often required that not only need to be large, but also need to have a very high degree of long-range spatial coherence. A standing wave lens array is perfectly suited to this because it has a very long coherence length (up to 30 km) due to the narrow frequency width of the laser required for the atom-optical focusing. Another example is the construction of a sensor array. Recent studies have found that nanostructures, just by the nature of their size and shape, can greatly enhance certain signals (an example of this is surface-enhanced Raman scattering[152]). Covering a large area with an array of identical nanostructures is thus a good way to make a very efficient sensor.

As a final example, we mention the possibility of using an array of dots or lines made by laser focusing in a standing wave as a nanoscale length standard. Because the standing-wave laser beam must be tuned to an atomic resonance for the pattern to be formed, the wavelength of the laser is determined with spectroscopic accuracy—that is, to better than a part per million, in the case of chromium. Thus the standing wave periodicity, which is simply half the wavelength

with some small corrections for wavefront curvature, is known with essentially the same accuracy. In the basic laser-focused deposition geometry (see section IV.A), the standing wave propagates parallel to the surface of the substrate, so its periodicity transfers directly to the deposited pattern, with some small corrections for angular deviations. The result is a deposited pattern that has an extremely accurate periodicity, or pitch, the major uncertainty of which is governed by the stability (thermal or other) of the substrate on which it is deposited.

These few examples concern applications of nanofabrication via atom optics assuming essentially a *status quo* of development, that is, assuming that only relatively incremental improvements will be added to the techniques already demonstrated. Taking a broader view, it is clear that there are many aspects of atomic manipulation that have not yet been brought to bear on nanofabrication. As research progresses, it is very likely that new, innovative ways will evolve applying some of the more recent atom manipulation techniques to the control of atoms as they impact a surface. With these new developments, it is quite possible that the ultimate capabilties of atom optics will be realized, focusing atoms with atomic resolution for unprecedented nanostructure fabrication.

1. See, e.g., F. B. Dunning, and R. G. Hulet (eds.), Atomic, Molecular and Optical Physics: Atoms and Molecules, Experimental Methods in the Physics Sciences, v. 29B, Academic Press, San Diego (1996).

2. N. Ramsey, Molecular Beams, Oxford University Press, London (1956).

3. L. I. Maissel and R. Glang (eds.), Handbook of Thin Film Technology, McGraw-Hill, New York (1970).

4. The presence of a v^3 factor in eq. (1) is a result of this being a *flux* distribution rather than a simple probability distribution. If the number density of atoms within a given velocity range is desired the factor should be v^2. Further discussion of this is found in reference [2], and also in F. Reif, Fundamentals of Statistical and Thermal Physics, McGraw-Hill, New York, (1965), pp 273-277. An interesting alternative treatment is found in C. C. Leiby, Jr and A. L. Besse, Am. J. Phys. **47**, 791 (1979).

5. Maissel, L. I. and Glang, R. (eds.) *op. cit.,* chapter 3.

6. G. K. Hubler (ed.), special issue "Pulsed laser deposition," Materials Research Society Bulletin, **17**, 26 (1992).

7. M. D. Morse, in Atomic, Molecular and Optical Physics: Atoms and Molecules, Experimental Methods in the Physics Sciences, F. B. Dunning, and R. G. Hulet (eds.), v. 29B, Academic Press, San Diego (1996), p 21.

8. T. G. Dietz, M. A. Duncan, D. E. Powers, and R. E. Smalley. J. Chem. Phys. **74**, 6511 (1981).

9. H. U. Hostettler and R. B. Bernstein, Rev. Sci. Instrum. **31**, 872 (1960).

10. W. M. Feist, (1968), in Electron Beam and Laser Beam Technology, L. Marton and A. B. El-Kareh (eds), Academic Press, New York, (1968), p. 1.

11. See e.g., E. E. Anderson, Modern Physics and Quantum Mechanics, W. B. Saunders, Philadelphia (1971), p. 317.

12. J. Prodan, A. Migdall, W. D. Phillips, L. So, H. Metcalf, and J. Dalibard, Phys. Rev. Lett. **54**, 992 (1985).

13. J. P. Gordon and A. Ashkin, Phys. Rev. A, **21**, 1606 (1980).

14. P. Meystre and S. Stenholm (eds.), Special issue "The mechanical effects of light," J. Opt. Soc. Am. B **2**, 1706 (1985).

15. S. Chu and C. Wieman (eds.), Special issue "Laser cooling and trapping of atoms," J. Opt. Soc. Am. B **6**, 2019 (1989).

16. J. Mlynek, V. Balykin, and P. Meystre (eds.), Special issue "Optics and interferometry with atoms," Appl. Phys. B **54**, 319 (1992).

17. C. S. Adams, M. Sigel, and J. Mlynek, Phys. Rep. **240**, 143 (1994).

18. A. Aspect, R. Kaiser, N. Vansteenkiste, and C. I. Westbrook, Physica Scripta **T58**, 69 (1995).

19. Y.-Z. Wang and L. Liu, Aust. J. Phys. **48**, 267 (1995).

20. C. C. Bradley and R. G. Hulet, in, Atomic, Molecular and Optical Physics: Atoms and Molecules, Experimental Methods in the Physics Sciences, v. 29B, F. B. Dunning and R. G. Hulet (eds.), Academic Press, San Diego (1996), p. 129.

21. C. S. Adams and E. Riis, Progress in Quantum Electronics, **21**, 1 (1997).

22. R. Loudon, The Quantum Theory of Light, Oxford University Press, Oxford (1973), pp.22-37.

23. W. D. Phillips and H. Metcalf, Phys. Rev. Lett. **48**, 596 (1982).

24. V. I. Balykin, V. S. Letokhov, and V. I. Mushin, *Pis'ma v Zhurnal Eksperimental'noi i Teoreticheskoi Fiziki* **29**, 614 (1979); W. Ertmer, R. Blatt, J. L. Hall, and M. Zhu, Phys. Rev. Lett. **54**, 996 (1985).

25. M. Zhu, C. W. Oates, and J. L. Hall, Phys. Rev. Lett. **67**, 46 (1991).

26. J. Dalibard and C. Cohen-Tannoudji (1985), J. Opt. Soc. Am. B **2**, 1706 (1985).

27. This phenomenon has been put to use to demonstrate an "optical Stern-Gerlach" effect. See T. Sleator, T. Pfau, V. Balykin, O. Carnal, and J. Mlynek, Phys. Rev. Lett. **68**, 1996 (1992).

28. R. Dum, P. Zoller, and H. Ritsch, Phys. Rev. A **45**, 4879 (1992).

29. J. Vanier and C. Audoin, Quantum Physics of Atomic Frequency Standards, Hilger, Bristol (1989).

30. M. H. Anderson, J. R. Ensher, M. R. Matthews, C. E. Wieman, and E. A. Cornell, Science **269**, 198 (1995).

31. T. Hänsch and A. Schawlow, Opt. Commun. **13**, 68 (1975); D. J. Wineland and W. M. Itano, Phys. Rev. A **20**, 1521 (1979).

32. S. Chu, L. Hollberg, J. E. Bjorkholm, A. Cable, and A. Ashkin, A. Phys. Rev. Lett. **55**, 48 (1985).

33. P. D. Lett, W. D. Phillips, S. L. Rolston, C. E. Tanner, R. N. Watts, C. I. Westbrook, J. Opt. Soc. Am. B **6**, 2084 (1989).

34. P. D. Lett, R. N. Watts, C. I. Westbrook, W. D. Phillips, P. L. Gould, and H. J. Metcalf, Phys. Rev. Lett. **61**, 169 (1988).

35. J. Dalibard and C. Cohen-Tannoudji, J. Opt. Soc. Am. B **6**, 2023 (1989).

36. P. Marte, R. Dum, R. Taïeb, P. D. Lett, and P. Zoller, Phys. Rev. Lett. **71**, 1335 (1993).

37. A. Aspect, E. Arimondo, R. Kaiser, N. Vansteenkiste, and C. Cohen-Tannoudji, Phys. Rev. Lett. **61**, 826 (1988).

38. A. Aspect, E. Arimondo, R. Kaiser, N. Vansteenkiste, and C. Cohen-Tannoudji, J. Opt. Soc. Am. B **6**, 2112 (1989).

39. M. Kasevitch and S. Chu, Phys. Rev. Lett. **69**, 1741 (1992).

40. A. L. Migdall, J. V. Prodan, W. D. Phillips, T. H. Bergeman, and H. J. Metcalf, Phys. Rev. Lett. **54**, 2596 (1985).

41. H. F. Hess, G. P. Kochanski, J. M. Doyle, N. Masuhara, D. Kleppner, and T. J. Greytak, Phys. Rev. Lett. **59**, 672 (1987).

42. J. J. Tollett, C. C. Bradley, C. A. Sackett, and R. G. Hulet, Phys. Rev. A **51**, R22 (1995).

43. E. L. Raab, M. Prentiss, A. Cable, S. Chu, and D. E. Pritchard, Phys. Rev. Lett. **59**, 2631 (1987).

44. A. M. Steane, M. Chowdhury, and C. J. Foot, J. Opt. Soc. Am. B **9**, 2142 (1992).

45. S. Chu, J. Bjorkholm, A. Ashkin, and A. Cable, Phys. Rev. Lett. **57**, 314 (1986).

46. J. D. Miller, R. A. Cline, and D. J. Heinzen, Phys. Rev. A **47**, R4567 (1993).

47. M. J. Renn, D. Montgomery, O. Vdovin, D. Z. Anderson, C. E. Wieman, and E. A. Cornell, Phys. Rev. Lett. **75**, 3253 (1995).

48. H. Ito, K. Sakaki, W. Jhe, and M. Ohtsu, Opt. Commun. **141**, 43 (1997).

49. S. N. Bose, Z. Phys. **26**, 178 (1924); A. Einstein, *Situnsber. Kgl. Preuss. Acad. Wiss*. **1924**, 261 (1924).

50. C. C. Bradley, C. A. Sackett, J. J. Tollet, and R. G. Hulet, Phys. Rev. Lett. **75**, 1687 (1995).

51. K. B. Davis, M.-O. Mewes, M. R. Andrews, N. J. van Druten, D. S. Durfee, D. M. Kurn, and W. Ketterle, Phys. Rev. Lett. **75**, 3969 (1995).

52. M.-O. Mewes, M. R. Andrews, D. M. Kurn, D. S. Durfee, C. G. Townsend, and W. Ketterle, Phys. Rev. Lett. **78**, 582 (1997).

53. V. I. Balykin and V. S. Letokhov, Physics Today **42**(4), 23 (1989).

54. See, e.g., E. Hecht, Optics, 2nd ed., Addison-Wesley, Reading, Massachusetts (1987), Ch. 5.

55. Electrostatic forces are typically too weak to form an atom lens because atoms do not have a permanent electric dipole moment. An electrostatic lens has been demonstrated for ammonia molecules, which do have a dipole moment. See J. P. Gordon, Phys. Rev. **99**, 1253 (1955).

56. H. Friedburg, Z. Phys. **130**, 493 (1951).

57. W. G. Kaenders, F. Lison, A. Richter, R. Wynands, and D. Meschede, Nature **375**, 214 (1995).

58. J. E. Bjorkholm, R. R. Freeman, A. Ashkin, and D. B. Pearson, Phys. Rev. Lett. **41**, 1361 (1978).

59. J. E. Bjorkholm, R. R. Freeman, A. Ashkin, and D. B. Pearson, Opt. Lett. **5**, 111 (1980).

60. V. I. Balykin and V. S. Letokhov, Opt. Commun. **64**, 151 (1987).

61. G. M. Gallatin and P. L. Gould, J. Opt. Soc. Am B **8**, 502 (1991).

62. J. J. McClelland, and M. R. Scheinfein, J. Opt. Soc. Am B **8**, 1974 (1991).

63. W. Glaser, Z. Phys. **117**, 285 (1941).

64. V. I. Balykin, V. S. Letokhov, Yu. B. Ovchinnikov, and A. I. Sidorov, J. Mod. Opt. **35**, 17 (1988).

65. T. Sleator, T. Pfau, V. Balykin, and J. Mlynek, Appl. Phys. B **54**, 375 (1992).

66. G. Timp, R. E. Behringer, D. M. Tennant, J. E. Cunningham, M. Prentiss, and K. K. Berggren, Phys. Rev. Lett. **69**, 1636 (1992).

67. J. J. McClelland, R. E. Scholten, E. C. Palm, and R. J. Celotta, Science **262**, 877 (1993).

68. R. W. McGowan, D. M. Giltner, and S. A. Lee, Opt. Lett. **20**, 2535 (1995).

69. U. Drodofsky, J. Stuhler, B.Brezger, T. Schulze, M. Drewsen, T. Pfau, and J. Mlynek, Microelectronic Engineering **35**, 285 (1997).

70. V. I. Balykin, V. V. Klimov, and V. S. Letokhov, J. Phys. II (France) **4**, 1981 (1994).

71. Qiming Li, K. G. H. Baldwin, H.-A. Bachor, and D. E. McClelland, J. Opt. Soc. Am. B **13**, 257 (1996).

72. O. Carnal, M. Sigel, T. Sleator, H. Takuma, and J. Mlynek, Phys. Rev. Lett. **67**, 3231 (1991).

73. K. K. Berggren, M. Prentiss, G. L. Timp, R. E. Behringer, J. Opt. Soc. Am. B **11**, 1166 (1994).

74. J. J. McClelland, J. Opt. Soc. Am. B **12**, 1761 (1995).

75. M. Drewsen, R. J. C. Spreeuw, and J. Mlynek, Opt. Commun. **125**, 77 (1996).

76. For extremely slow atoms, whose De Broglie wavelength is much larger than the distance over which the surface interaction potential changes, the sticking probability will go to zero due to quantum reflection. See, e.g., J. Boheim, W. Brenig, and J. Stutzki, Z. Physik B **48**, 43 (1982).

77. T. Roach, H. Abele, M. G. Boshier, H. L. Grossman, K. P. Zetie, and E. A. Hinds, Phys. Rev. Lett. **75**, 629 (1995).

78. A. I. Sidorov, R. J. McLean, W. J. Rowlands, D. C. Lau, J. E. Murphy, M. Walkiewicz, G. I. Opat, and P. Hannaford, Quantum and Semiclass. Opt. **8**, 713 (1996).

79. R. J. Cook and R. K. Hill, Opt. Commun. **43**, 258 (1982).

80. M. A. Kasevich, D. S. Weiss, and S. Chu, Opt. Lett. **15**, 607 (1990).

81. C. G. Aminoff, A. M. Steane, P. Bouyer, P. Desbiolles, J. Dalibard, and C. Cohen-Tannoudji, Phys. Rev. Lett. **71**, 3083 (1993).

82. A. Landragin, G. Labeyrie, C. Henkel, R. Kaiser, N. Vansteenkiste, C. I. Westbrook, and A. Aspect, Opt. Lett. **21**, 1591 (1996).

83. V. I. Balykin, V. S. Letokhov, Yu. B. Ovchinnikov, and A. I. Sidorov, Phys. Rev. Lett. **60**, 2137 (1988).

84. W. Seifert, C. S. Adams, V. I. Balykin, C. Heine, Yu. Ovchinnikov, and J. Mlynek, Phys. Rev. A **49**, 3814 (1994).

85. D. R. Frankl, Prog. Surf. Sci. **13**, 285 (1983).

86. J. H. Muller, D. Bettermann, V. Rieger, F. Ruschewitz, K. Sengstock, U. Sterr, M. Christ, M. Schiffer A. Scholtz, and W. Ertmer, AIP conference proceedings (14th International Conference on Atomic Physics, Boulder, CO, 31 July – 5 August 1994), **323**, 240 (1996).

87. See, e.g., P. Berman (ed.), Atom Interferometry, Academic Press, San Diego, (1997).

88. D. W. Keith, M. L. Schattenberg, H. I. Smith, and D. E. Pritchard, Phys. Rev. Lett. **61**, 1580 (1988).

89. O. Carnal, A. Faulstich, and J. Mlynek, Appl. Phys. B **53**, 88 (1991).

90. J. F. Clauser, and Shifang Li, Phys. Rev. A **49**, R2213 (1994)..

91. M. S. Chapman, C. R. Ekstrom, T. D. Hammond, J. Schmiedmayer, B. E. Tannian, S. Wehinge, and D. E. Pritchard, Phys. Rev. A **51**, R14 (1995).

92. J. Fujita, M. Morinaga, T. Kishimoto, M. Yasuda, S. Matsui, and F. Shimizu, Nature, **380**, 691 (1996).

93. M. Morinaga, M.Yasuda, T. Kishimoto, F. Shimizu, J. Fujita, and S. Matsui, Phys. Rev. Lett. **77**, 802 (1996).

94. P. L. Gould, G. A. Ruff, and D. E. Pritchard, Phys. Rev. Lett. **56**, 827 (1986).

95. P. J. Martin, B. G. Oldaker, A. H. Miklich, and D. E. Pritchard, Phys. Rev. Lett. **60**, 515 (1988).

96. T. Pfau, Ch. Kurtsiefer, C. S. Adams, M. Sigel, and J. Mlynek, Phys. Rev. Lett. **71**, 3427 (1993).

97. K. S. Johnson, A. Chu, T. W. Lynn, K. K. Berggren, M. S. Shahriar, and M. Prentiss, Opt. Commun. **20**, 1310 (1995).

98. E. M. Rasel, M. K. Oberthaler, H. Batelaan, J. Schmiedmayer, and A. Zeilinger, Phys. Rev. Lett. **75**, 2633 (1995).

99. D. M. Giltner, R. W. McGowan, and S. A. Lee, Phys. Rev. A **52**, 3966 (1995).

100. J. V. Hajnal and G. I. Opat, Opt. Commun. **71**, 119 (1989).

101. M. Christ, A. Scholz, M. Schiffer, R. Deutschmann, and W. Ertmer, Opt. Commun. **107**, 211 (1994).

102. R. Brouri, R. Asimov, M. Gorlicki, S. Feron, J. Reinhardt, V. Lorent, and H. Haberland, Opt. Commun. **124**, 448 (1996).

103. For an electron-optical discussion, see O. Klemperer, Electron Optics, 2nd ed., Cambridge University Press, London (1953), pp. 12-15; for a light-optical discussion, see M. Born and E. Wolf, Principles of Optics, 3rd ed., Pergamon Press, Oxford (1965), pp.166-169.

104. B. Sheehy, S.-Q. Shang, R. Watts, S. Hatamian, and H. Metcalf, J. Opt. Soc. Am. B **6**, 2165 (1989).

105. V. I. Balykin, V. S. Letokhov, and A. I. Sidorov, *Pis'ma Zh. Eksp. Teor. Fiz.* **40**, 251 (1984).

106. C. E. Tanner, B. P. Masterson, and C. E. Wieman, Opt. Lett. **13**, 357 (1988).

107. V. I. Balykin, V. S. Letokhov, Yu. B. Ovchinnikov, and S. V. Shul'ga, Opt. Commun. **77**, 152 (1990).

108. W. Rooijakkers, W. Hogervorst, and W. Vassen, Opt. Commun. **123**, 321 (1996).

109. A. Aspect, J. Dalibard, A. Heidmann, C. Salomon, and C. Cohen-Tannoudji, Phys. Rev. Lett. **57**, 1688 (1986).

110. Y. Wang, Y. Cheng, and W. Cai, Opt. Commun. **70**, 462 (1989).

111. R. E. Scholten, R. Gupta, J. J. McClelland, and R. J. Celotta, Phys. Rev. A **55**, 1331 (1997).

112. E. Riis, D. S. Weiss, K. A. Moler, and S. Chu, Phys. Rev. Lett. **64**, 1658 (1990).

113. J. Yu, J. Djemaa, P. Nosbaum, and P. Pillet, Opt. Commun. **112**, 136 (1994).

114. M. D. Hoogerland, J. P. J. Driessen, E. J. D. Vredenbregt, H. J. L. Megens, M. P. Schuwer, H. C. W. Beijerinck, and K. A. H. van Leeuwen, Appl. Phys. B **62**, 323 (1996).

115. S. V. Andreev, V. I. Balykin, V. S. Letokhov, and V. G. Minogin, *Pis'ma Zh. Eksp. Teor. Fiz.* **34**, 463 (1981).

116. W. D. Phillips, J. V. Prodan, and H. J. Metcalf, J. Opt. Soc. Am. B **2**, 1751 (1985).

117. J. Nellsen, J. H. Müller, K. Sengstock, and W. Ertmer, J. Opt. Soc. Am. B **6**, 2149 (1989).

118. A. Faulstich, A. Schnetz, M. Sigel, T. Sleator, O. Carnal, V. Balykin, H. Takuma, and J. Mlynek, Europhys. Lett. **17**, 393 (1992).

119. J. J. McClelland and M. H. Kelley, Phys. Rev. A **31**, 3704 (1985).

120. M. Prentiss, G. Timp, N. Bigelow, R. E. Behringer, and J. E. Cunningham, Appl. Phys. Lett. **60**, 1027 (1992).

121. V. Natarajan, R. E. Behringer, D. M. Tennant, and G. Timp, J. Vac. Sci. Technol. B **13**, 2823 (1995).

122. R. E. Behringer, V. Natarajan, and G. Timp, Appl. Phys. Lett. **68**, 1034 (1996).

123. R. E. Behringer, V. Natarajan, and G. Timp, Appl. Surf. Sci. **104/105**, 291 (1996).

124. V. Natarajan, R. E. Behringer, and G. Timp, Phys. Rev. A **53**, 4381 (1996).

125. R. E. Behringer, V. Natarajan, G. Timp, and D. M. Tennant, J. Vac. Sci. Technol. B **14**, 4072 (1996).

126. J. J. McClelland, R. Gupta, Z. J. Jabbour, and R. J. Celotta, Aust. J. Phys. **49**, 555 (1996).

127. R. E. Scholten, J. J. McClelland, E. C. Palm, A. Gavrin, and R. J. Celotta, J. Vac. Sci. Technol. B **12**, 1847 (1994).

128. R. J. Celotta, R. Gupta, R. E. Scholten, and J. J. McClelland, J. Appl. Phys. **79**, 6079 (1996).

129. U. Drodofsky, J. Stuhler, B. Brezger, Th. Schulze, M. Drewsen, T. Pfau, and J. Mlynek, Microelectronic Engineering **35**, 285 (1997).

130. R. Gupta, J. J. McClelland, Z. J. Jabbour, and R. J. Celotta, Appl. Phys. Lett. **67**, 1378 (1995).

131. U. Drodofsky, J. Stuhler, Th. Schulze, M. Drewsen, B. Brezger, T. Pfau, and J. Mlynek, Appl. Phys. B **65**, 755 (1997).

132. R. Gupta, J. J. McClelland, P. Marte, and R. J. Celotta, Phys. Rev. Lett. **76**, 4689 (1996).

133. Y. Xia, J. J. McClelland, R. Gupta, D. Qin, X.-M. Zhao, L. L. Sohn, R. J. Celotta, and G. M. Whitesides, Adv. Mater. **9**, 147 (1997).

134. D. A. Tulchinsky, M. H. Kelley, J. J. McClelland, R. Gupta, and R. J. Celotta, J. Vac. Sci. Technol. A, in press (1998).

135. M. R. Scheinfein, J. Unguris, M. H. Kelley, D. T. Pierce, and R. J. Celotta, Rev. Sci. Instrum. **60**, 1 (1989).

136. J. J. McClelland, R. Gupta, R. J. Celotta, and G. A. Porkolab, Appl. Phys. B, in press (1997).

137. The value of 57 mW/cm^2 is calculated assuming a two-level atom. In McGowan *et al.*, Opt. Lett. **20**, 2535 (1995), the value quoted is 140 mW/cm^2, which is an effective saturation intensity taking into account linearly polarized excitation of several magnetic sublevels having Clebsch-

Gordan coefficients less than unity.

138. J. Chen, J. G. Story, and R. G. Hulet, Phys. Rev. A **47**, 2128 (1993).

139. T. Bergeman, Phys. Rev. A **48**, R3425 (1993).

140. A. P. Chu, K. K. Berggren, K. S. Johnson, and M. G. Prentiss, Quantum and Semiclassical Optics **8**, 521 (1996).

141. K. K. Berggren, A. Bard, J. L. Wilbur, J. D. Gillaspy, A. G. Helg, J. J. McClelland, S. L. Rolston, W. D. Phillips, M. Prentiss, and G. M. Whitesides, Science **269**, 1255 (1995).

142. S. Nowak, T. Pfau, and J. Mlynek, Appl. Phys. B **63**, 203 (1996).

143. A. Bard, K. K. Berggren, J. L. Wilbur, J. D. Gillaspy, S. L. Rolston, J. J. McClelland, W. D. Phillips, M. Prentiss, and G. M. Whitesides, J. Vac. Sci. Technol. B **15**, 1805 (1997).

144. K. S. Johnson, K. K. Berggren, A. Black, C. T. Black, A. P. Chu, N. H. Dekker, D. C. Ralph, J. H. Thywissen, R. Younkin, M. Tinkham, M. Prentiss, and G. M. Whitesides, Appl. Phys. Lett. **69**, 2773 (1996).

145. S. J. Rehse, A. D. Glueck, S. A. Lee, A. B. Goulakov, C. S. Menoni, D. C. Ralph, K. S. Johnson, and M. Prentiss, Appl. Phys. Lett. **71**, 1427 (1997).

146. M. Kreis, F. Lison, D. Haubrich, D. Meschede, S. Nowak, T. Pfau, and J. Mlynek, Appl. Phys. B **63**, 649 (1996).

147. K. K. Berggren, R. Younkin, E. Cheung, M. Prentiss, A. J. Black, G. M. Whitesides, D. C. Ralph, C. T. Black, and M. Tinkham, Adv. Materials **9**, 52 (1997).

148. R. Younkin, K. K. Berggren, K. S. Johnson, M. Prentiss, D. C. Ralph, and G. M. Whitesides, Appl. Phys. Lett. **71**, 1261 (1997).

149. F. Lison, H.-J. Adams, D. Haubrich, M. Kreis, S. Nowak, and D. Meschede, Appl. Phys. B **65**, 419 (1997).

150. K. J. Ross and B. Sonntag. Rev. Sci. Instrum. **66**, 4409 (1995).

151. W. L. Weise, M. W. Smith, and B. M. Glennon, NSRDS-NBS **4**, (1966); W. L. Weise, M. W. Smith, and B. M. Miles, NSRDS-NBS **22**, (1969); G. A. Martin, J. R. Fuhr, and W. L. Weise, J. Phys. Chem. Ref. Data **17**, Suppl. 3 (1988); J. R. Fuhr, G. A. Martin, and W. L. Weise, J. Phys. Chem. Ref. Data **17**, Suppl. 4 (1988); see also world wide web site *http://aeldata.phy.nist.gov/nist_atomic_spectra.html*.

152. A. Otto, I. Mrozek, H. Grabhorn, W. Akemann, J. Physics: Condensed Matter **4**, 1143

(1992).